PLOS PATHOGENS

RESEARCH ARTICLE

Transcriptional suppression of sphingolipid catabolism controls pathogen resistance in *C. elegans*

Mohamad A. Nasrallah[1☯], Nicholas D. Peterson[1☯], Elizabeth S. Szumel[1], Pengpeng Liu[2], Amanda L. Page[1], Samantha Y. Tse[1], Khursheed A. Wani[1], Claire E. Tocheny[1], Read Pukkila-Worley[1]*

1 Program in Innate Immunity, Division of Infectious Diseases and Immunology, Department of Medicine, University of Massachusetts Chan Medical School, Worcester, Massachusetts, United States of America, **2** Department of Molecular, Cell and Cancer Biology, University of Massachusetts Chan Medical School, Worcester, Massachusetts, United States of America

☯ These authors contributed equally to this work.
* Read.Pukkila-Worley@umassmed.edu

Citation: Nasrallah MA, Peterson ND, Szumel ES, Liu P, Page AL, Tse SY, et al. (2023) Transcriptional suppression of sphingolipid catabolism controls pathogen resistance in *C. elegans*. PLoS Pathog 19(10): e1011730. https://doi.org/10.1371/journal.ppat.1011730

Editor: Nina R. Salama, Fred Hutchinson Cancer Research Center, UNITED STATES

Received: August 18, 2023

Accepted: October 1, 2023

Published: October 31, 2023

Data Availability Statement: The mRNA-seq and ChIP-seq datasets were deposited in the NCBI Gene Expression Omnibus, a publicly available database, using the Accession numbers GSE240425 and GSE240426, respectively. All other data is available in this manuscript. S1 Table contains the source data for the RNAi screen. S5 and S6 Tables contain all other source data and statistical tests used in this manuscript.

Funding: Salary for the indicated individuals and the research was supported by R01 AI130289 (to

Abstract

Sphingolipids are required for diverse biological functions and are degraded by specific catabolic enzymes. However, the mechanisms that regulate sphingolipid catabolism are not known. Here we characterize a transcriptional axis that regulates sphingolipid breakdown to control resistance against bacterial infection. From an RNAi screen for transcriptional regulators of pathogen resistance in the nematode *C. elegans*, we identified the nuclear hormone receptor *nhr-66*, a ligand-gated transcription factor homologous to human hepatocyte nuclear factor 4. Tandem chromatin immunoprecipitation-sequencing and RNA sequencing experiments revealed that NHR-66 is a transcriptional repressor, which directly targets sphingolipid catabolism genes. Transcriptional de-repression of two sphingolipid catabolic enzymes in *nhr-66* loss-of-function mutants drives the breakdown of sphingolipids, which enhances host susceptibility to infection with the bacterial pathogen *Pseudomonas aeruginosa*. These data define transcriptional control of sphingolipid catabolism in the regulation of cellular sphingolipids, a process that is necessary for pathogen resistance.

Author summary

Individual micronutrients and metabolites are essential for animals to survive challenge with infectious pathogens. Defining the metabolic requirements for pathogen resistance is therefore important to understand the links between nutrient acquisition, metabolism and host susceptibility to bacterial infection. Here we demonstrate that the cellular regulation of sphingolipids, complex macromolecules that are required for diverse biological processes, is required for the nematode *C. elegans* to survive infection with the pathogen *Pseudomonas aeruginosa*. We show that the *C. elegans* nuclear hormone receptor NHR-66, a ligand-gated transcription factor, directly regulates sphingolipid catabolism by repressing the transcription of two enzymes, sphingosine phosphate lyase (SPL-2) and acid ceramidase (ASAH-2). Transcriptional repression of these catabolic enzymes by

R.P.W.), R01 AI159159 (to R.P.W.), a diversity supplement to R01 AI159159 (to M.A.N. and R.P.W.), R21 AI163430 (to R.P.W.), F30 AI150127 (to N.D.P.), F30 DK127690 (to S.Y.T.), T32 AI132152 (to N.D.P.), T32 AI095213 (to S.Y.T.), and T32 GM107000 (to M.A.N., N.D.P. and S.Y.T.). The funders had no role in study design, data collection and analysis, decision to publish, or preparation of the manuscript.

Competing interests: The authors have declared that no competing interests exist.

NHR-66 controls the levels of sphingolipids in the cell in a manner that is required for host survival during pathogen challenge.

Introduction

Sphingolipids are required for the integrity, fluidity, and barrier function of cell membranes. Sphingolipids are also metabolized to bioactive signaling molecules, such as sphingosine-1-phosphate, that have been implicated in fibrosis, cell proliferation, neurotransmission, and immune-cell trafficking [1–8]. In addition, ceramides, a sub-class of sphingolipids, are important for apoptosis, response to cellular stress, and innate immunity [9–16]. Sphingolipid levels are therefore tightly regulated by specific biosynthetic and catabolic pathways.

Ceramides and other sphingolipids are broken down in cells by specific enzymes. For example, acid ceramidase catabolizes ceramides to sphingosines, which can be recycled back to ceramides or phosphorylated to produce bioactive lipids [17]. The final exit point of sphingolipid catabolism is the irreversible breakdown of sphingosine-1-phosphate into long-chain fatty acid aldehyde and phospho-ethanolamine by sphingosine phosphate lyase [2]. Importantly, several human inborn errors of metabolism, such as Tay-Sachs and Niemann-Pick diseases, are caused by defects in the breakdown of sphingolipids [18–20]. Although the biochemical steps in sphingolipid and ceramide catabolism are defined, it is not known how these processes are regulated and whether such mechanisms contribute to stress resistance.

Gene regulatory networks sense metabolic perturbations in the cell and regulate the flux of cellular metabolites by changing the transcription of specific enzymes [21,22]. A few specific examples of such metabolic gene regulatory networks have been characterized, particularly in the regulation of specific metabolites, lipids, and cholesterol, which promote adaptation to diet or changing environmental conditions [23–30]. Many of these networks utilize nuclear hormone receptors (NHRs), which are ligand-gated transcription factors that regulate cellular physiology by controlling gene expression. The nematode *Caenorhabditis elegans* has been particularly useful for characterizing metabolic gene regulatory networks, in part because its genome encodes a large number of *nhr* genes compared to other metazoans. Nematodes express 274 NHRs compared to 42 in humans and 24 in *Drosophila*, the great majority of which have unknown functions [31–35]. Intriguingly, of the few *C. elegans* NHRs that have been characterized in detail, several have specialized functions in pathogen detection or immunometabolism. For example, one *C. elegans* NHR, NHR-86, surveys for a pathogen-derived metabolite—a "pattern of pathogenesis" specifically associated with infection or bacterial virulence—to assess the relative threat of a bacterial pathogen in its environment and activate host immune defenses [36]. Other *C. elegans nhr* genes regulate metabolism to promote survival during pathogen infection. The *C. elegans* peroxisome proliferator-activated receptor α (PPARα) homolog NHR-49 is a master regulator of lipid metabolism and *nhr-49* mutants are dramatically hypersusceptible to killing by bacterial pathogens [37,38]. Likewise, the monounsaturated fatty acid oleate and the methyl donor S-adenosylmethionine, whose levels are each regulated by NHR-49, are individually necessary to survive pathogen challenge [39,40]. In addition, control of cellular cholesterol levels by NHR-8, a *C. elegans* homolog of mammalian liver X receptor and pregnane X receptor, primes protective activation of the p38 PMK-1 innate immune pathway [41] and is required for pathogen resistance [41,42]. Nuclear hormone receptors also suppress the transcription of innate immune defense genes to promote immune homeostasis, both downstream of a key defense regulator [43] and via a response linked to iron uptake [44]. Together, these studies characterize novel mechanisms of

immunometabolism [45] and suggest that the NHR family in *C. elegans* may have expanded, at least in part, because of their diverse roles in promoting survival during pathogen infection.

Here, we demonstrated that regulation of sphingolipid breakdown occurs at the transcriptional level and showed that this process is required for pathogen resistance in *C. elegans*. We discovered that NHR-66 suppresses sphingolipid catabolism by directly repressing the transcription of two enzymes: sphingosine phosphate lyase (*spl-2*) and acid ceramidase (*asah-2*). Transcriptional de-repression of *spl-2* and *asah-2* in *nhr-66* loss-of-function mutants drove the excessive breakdown of sphingolipids and ceramides, which compromised host survival during pathogen infection. These data demonstrated for the first time that transcriptional regulation of sphingolipid catabolism is required for pathogen resistance, revealing a novel pathway that can be targeted to promote survival during bacterial infection.

Results

An RNAi screen identifies nuclear hormone receptors required for pathogen resistance in *C. elegans*

We performed an RNAi screen to identify the *C. elegans nhr* genes required for host survival during bacterial infection (Fig 1A). From a primary screen of 271 of the 274 *nhr* genes in the *C. elegans* genome, we identified 15 *nhr* genes that, when knocked down, reduced *C. elegans* survival during infection with the bacterial pathogen *P. aeruginosa* (Fig 1A and 1C and S1 Table). Lifespan assays, performed by monitoring survival of nematodes fed on a standard bacterial diet (*E. coli* OP50), revealed that 10 of these 15 *nhr* genes affected pathogen susceptibility, but without pleiotropic effects on nematode lifespan (Fig 1B and 1C and S1 Table). We then performed three independent trials of *P. aeruginosa* pathogenesis assays in *C. elegans* following RNAi-mediated knockdown of these 10 *nhr* genes (S1A Fig and S1 Table). RNAi targeting four of these *nhr* genes (*nhr-8*, *nhr-66*, *nhr-31*, and *nhr-32*) rendered *C. elegans* hypersusceptible to pathogen-mediated killing in three of three biological replicate trials (S1A Fig and S1 Table).

Loss-of-function mutants in three of these four *nhr* genes died significantly faster than wild-type animals during bacterial infection (Figs 1D, 1E, S1B and S1C). The *nhr-31(tm1547)* mutant is embryonically lethal [46]. We confirmed that mutations at these specific loci led to pathogen hypersusceptibility by re-introducing a wild-type copy of each of these *nhr* genes, expressed under the control of their own promoters, into the *nhr-8(hd117)*, *nhr-32(gk810)*, and *nhr-66(ok940)*, loss-of-function mutant backgrounds. Complementation of *nhr-8* (S1D Fig) [42], *nhr-32* (S1E Fig), and *nhr-66* (Fig 1E) in this manner restored wild-type resistance to pathogen infection. Thus, *nhr-8*, *nhr-32*, and *nhr-66* specifically and robustly enhance *C. elegans* survival during *P. aeruginosa* infection.

The recovery of *nhr-8* provided an internal control for the RNAi screen, as we previously characterized its role in immune regulation and pathogen resistance [41]. Likewise, *nhr-49* is required for normal lifespan in *C. elegans* and resistance to pathogen infection [37,38,47,48], findings we also observed (Fig 1C). We chose 12 *nhr* genes that were not recovered in our primary screen and confirmed that knockdown of these genes did not affect resistance to *P. aeruginosa* infection (S1F Fig). Together, these results validated the RNAi screen, which identified specific *C. elegans nhr* genes that are required for resistance to *P. aeruginosa* infection.

NHR-66 is a transcriptional repressor that directly targets stress response and sphingolipid metabolism genes

To further characterize the role of NHR-66 in promoting resistance to pathogen infection, we performed chromatin immunoprecipitation sequencing (ChIP-seq) and RNA sequencing

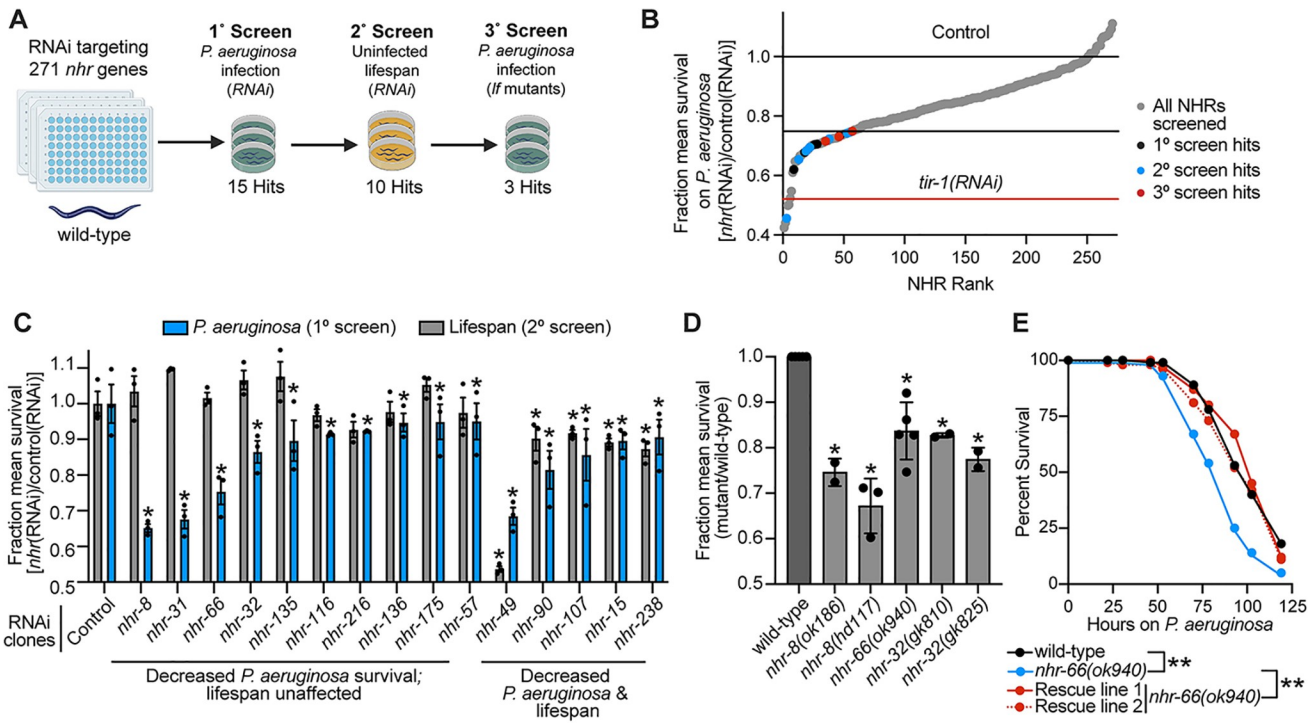

Fig 1. An RNAi screen identifies nuclear hormone receptors required for pathogen resistance in *C. elegans*. **A.** A schematic of the RNAi screen for 271 of the 274 *nhr* genes that control resistance to *P. aeruginosa* infection in *C. elegans* is shown. **B.** The fraction mean survival compared to wild-type animals on *P. aeruginosa* is plotted for each of the *C. elegans nhr* RNAi clones in the screen. Hits from the primary, secondary, and tertiary screens are indicated. The fraction mean survival for the control *tir-1(RNAi)* is shown. **C.** The fraction mean survival during *P. aeruginosa* infection and in a lifespan assay is compared for each of the 15 *nhr* genes that were identified in the primary screen. Data are the average of three replicate trials with error bars showing SEM (n = 3) with error bars representing SEM. * equals $p<0.05$ (Kaplan-Meier method with log-rank test). **D.** The fraction mean survival during *P. aeruginosa* infection was plotted for the indicated mutant genotypes. Mean survival is the average of 2–5 biological replicates and is expressed relative to the survival of wild-type *C. elegans*, with error bars representing SEM. * equals $p<0.05$ (Kaplan-Meier method with log-rank test). **E.** *C. elegans-P. aeruginosa* pathogenesis assay with *C. elegans* of the indicated genotypes. The difference in survival between *nhr-66(ok940)* and the other genotypes is significant ** $p<0.01$ (log-rank test, n = 3). Data shown are representative of three independent trials. Sample sizes, mean lifespan, and p-values for each trial are shown in S5 Table. The source data for the RNAi screen is in S1 Table. See also S1 Fig. Fig 1A was made using BioRender.

https://doi.org/10.1371/journal.ppat.1011730.g001

(RNA-seq). For these experiments, we used CRISPR-Cas9 to insert a 3xFLAG sequence at the *nhr-66* locus (S2A Fig). NHR-66 protein-DNA complexes were precipitated using an anti-FLAG antibody and deep sequenced. In parallel, mRNA transcripts were quantified in *nhr-66* (*ok940*) mutant and wild-type animals. A comparison of the ChIP-seq and RNA-seq datasets revealed that NHR-66 bound to the promoters and regulated the transcription of 18 genes (Fig 2A and 2E and S2 and S3 Tables). We validated the ChIP-seq data using PCR to determine enrichment of promoter sequences of three NHR-66 targets [*spl-2* (Fig 2F), *asah-2* (Fig 2G), and *cyp-13A4* (Fig 2H)] from biological replicate ChIP samples (ChIP-PCR). In addition, immunoprecipitation with an anti-FLAG antibody did not enrich for random intergenic regions in NHR-66:FLAG animals, as measured by ChIP-seq (Fig 2I) or ChIP-PCR (Fig 2J and 2K). The RNA-seq dataset was validated using qRT-PCR to measure the expression of *spl-2* (S2B Fig), *asah-2* (S2C Fig), and *cyp-13A4* (S2D Fig).

Interestingly, 16 of the 18 NHR-66 targets were expressed at higher levels in *nhr-66(ok940)* mutants than in wild-type (Fig 2B). Thus, NHR-66 is predominantly a transcriptional repressor. In addition, NHR-66 directly promotes its own transcription, suggesting that it functions in a feedback loop (Fig 2B). Two of the 18 NHR-66 transcriptional targets, *spl-2* and *asah-2*, function in sphingolipid catabolism [49] and eight are stress or pathogen response genes.

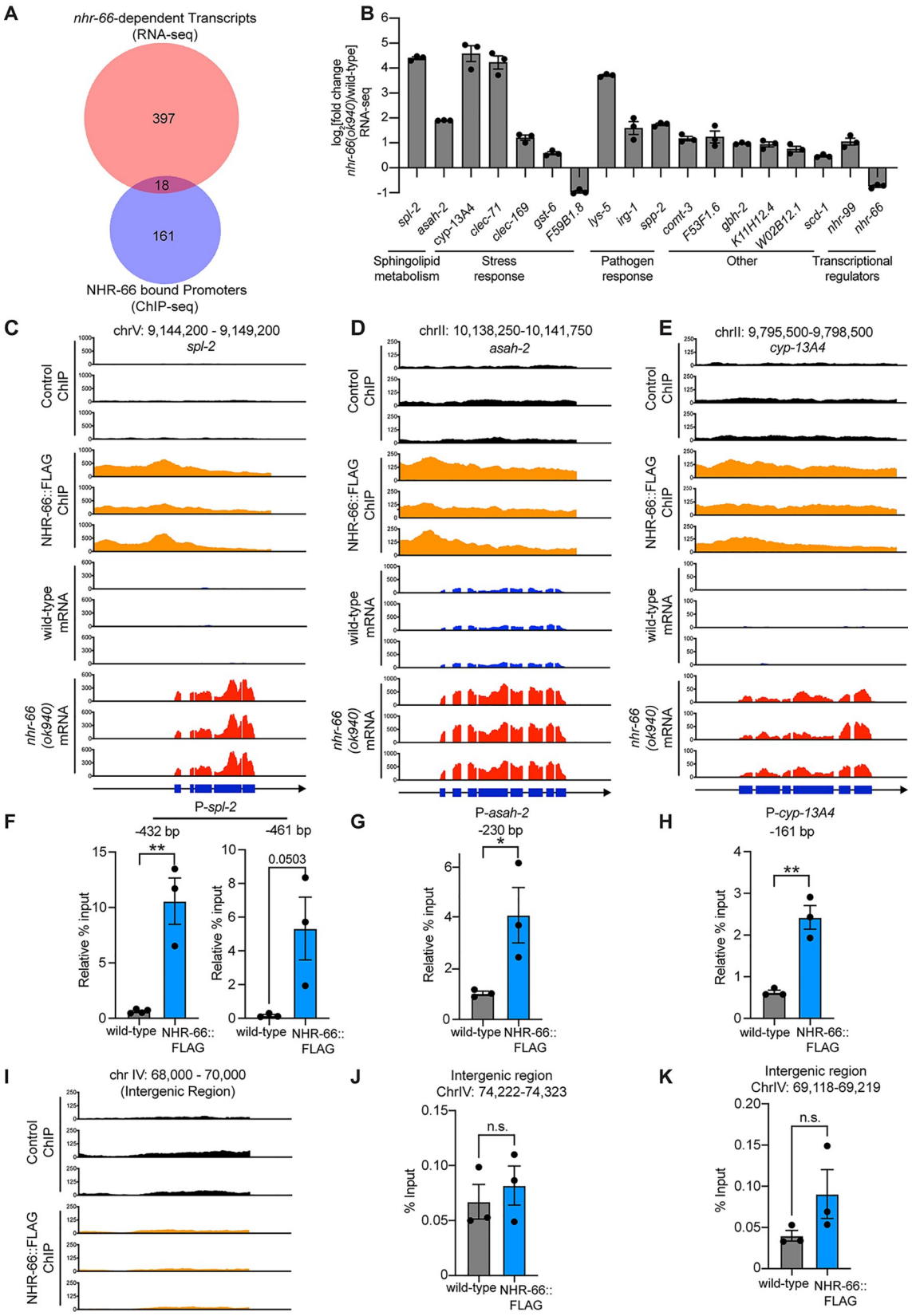
A
nhr-66-dependent Transcripts
(RNA-seq)
397
18
161
NHR-66 bound Promoters
(ChIP-seq)
B
log2[fold change
nhr-66(ok940)/wild-type]
RNA-seq
spl-2
asah-2
cyp-13A4
clec-71
clec-169
gst-6
F59B1.8
lys-5
irg-1
spp-2
comt-3
F53F1.6
gbh-2
K11H12.4
W02B12.1
scd-1
nhr-99
nhr-66
Sphingolipid metabolism
Stress response
Pathogen response
Other
Transcriptional regulators
C
chrV: 9,144,200 - 9,149,200
spl-2
Control ChIP
NHR-66::FLAG ChIP
wild-type mRNA
nhr-66 (ok940) mRNA
D
chrII: 10,138,250-10,141,750
asah-2
E
chrII: 9,795,500-9,798,500
cyp-13A4
F
P-spl-2
-432 bp
-461 bp
Relative % input
0.0503
wild-type
NHR-66:: FLAG
G
P-asah-2
-230 bp
H
P-cyp-13A4
-161 bp
I
chr IV: 68,000 - 70,000
(Intergenic Region)
J
Intergenic region
ChrIV: 74,222-74,323
% Input
n.s.
K
Intergenic region
ChrIV: 69,118-69,219

Fig 2. NHR-66 is a transcriptional repressor that directly targets stress response and sphingolipid metabolism genes. A. Venn diagram showing the overlap between the genes whose promoters were bound by NHR-66::FLAG in the ChIP-seq experiment and the genes that are differentially regulated in *nhr-66(ok940)* mutants compared to wild-type (from the RNA-seq experiment). The overlap between these datasets is significant (hypergeometric p-value = 1.42 x 10^{-3}). For both the RNA-seq and ChIP-seq experiments, n = 3 biological replicates, q<0.01. **B.** Fold change in expression of the 18 direct target genes of NHR-66 in *nhr-66*(*ok940*) mutants compared to wild-type animals is shown from the RNA-seq data. n = 3 biological replicates, q<0.01. **C–E.** ChIP-seq and mRNA-seq profiles from each of the three biological replicates are presented for *spl-2* (C), *asah-2* (D), and *cyp-13A4* (E). The y-axis is the number of reads (log_2). A gene model shows the location of the exons (blue) of the indicated genes. **F and G.** ChIP-PCR, performed to confirm the ChIP-seq data, is shown. The % input relative to the abundance of a random intergenic region of chromosome IV is presented for the promoter regions of *spl-2* (F) (two different regions are shown), *asah-2* (G) and *cyp-13A4* (H) (locations are indicated relative to the start codon of the gene). ChIP-seq profiles **(I)** and ChIP-PCR data **(J and K)** are shown for random intergenic regions on chromosome IV, as described above. For the ChIP-PCR data in this figure, n = 3 biological replicates, $^{*}p<0.05$ and $^{**}p<0.01$ (Student's unpaired t-test). Source data for this figure is in S6 Table. See also S2 Table for the RNA-seq data, S3 Table for the ChIP-seq data, and S2 Fig.

https://doi.org/10.1371/journal.ppat.1011730.g002

Thus, NHR-66 binds to the promoters of stress response and sphingolipid metabolism genes to repress their transcription.

NHR-66 suppresses intestinal sphingolipid catabolism genes to promote resistance to *P. aeruginosa* infection

Given that both *spl-2* and *asah-2* are transcriptionally suppressed by NHR-66, we hypothesized that regulation of sphingolipid breakdown by NHR-66 is required for pathogen resistance in *C. elegans* and that hyperactivation of these enzymes accounts for the hypersusceptibility of *nhr-66(ok940)* mutants to pathogen infection. To test this hypothesis, we used RNAi to knockdown the NHR-66 target genes *spl-2* and *asah-2* in the *nhr-66(ok940)* mutant background. Importantly, RNAi of both *spl-2* (Fig 3A and 3B) and *asah-2* (Fig 3C and 3D) restored wild-type susceptibility to pathogen infection. qRT-PCR of *spl-2* (Fig 3B) and *asah-2* (Fig 3D) confirmed that RNAi depleted these transcripts in the *nhr-66(ok940)* mutant animals.

We next asked in which tissue NHR-66 functions to repress sphingolipid catabolism and promote pathogen resistance. We generated a transcriptional reporter for the NHR-66 target, *spl-2*, by fusing its promoter to *gfp* (*spl-2*p::*gfp*). In the *nhr-66(ok940)* mutant, *spl-2*p::*gfp* was strongly induced and expressed in the intestinal epithelium (Fig 3E). Consistent with these data, RNAi-mediated knockdown of *nhr-66* specifically in the intestine, using a *C. elegans* strain engineered to perform RNAi selectively in this tissue, increased the expression of *spl-2* (Fig 3F), as well as two other NHR-66 targets [*asah-2* (Fig 3G) and *cyp-13A4* (Fig 3H)]. In addition, knockdown of *nhr-66* in the intestine rendered *C. elegans* hypersusceptible to *P. aeruginosa* infection (Fig 3I). However, knockdown of *nhr-66* using a strain engineered to perform RNAi only in the hypodermis conferred only a subtle hypersusceptibility to pathogen infection (Fig 3J). Of note, we previously tested the efficiency of RNAi in these engineered strains and found that *C. elegans* MGH167, the strain used for intestinal-specific RNAi, performs RNAi in the intestine, and not in the hypodermis, body wall muscle or germline [50]. Conversely, RNAi in *C. elegans* JM43, the strain used for hypodermal-specific RNAi, is still able to perform RNAi in the intestine, body wall muscle and germline, but not as efficiently as in the hypodermis [50]. Thus, in the *C. elegans* JM43 background, "off-target" RNAi-mediated knockdown of *nhr-66* in the intestine may account for the observed subtle enhancement of susceptibility to bacterial infection (Fig 3J). Additionally, we observed that *C. elegans nhr-66 (ok940)* mutants accumulated more *P. aeruginosa* in their intestines than wild-type animals, consistent with the enhanced susceptibility of this mutant to pathogen infection (Fig 3K). Together, these data indicate that NHR-66 functions in the intestine to suppress the transcription of sphingolipid catabolism genes and promote pathogen resistance.

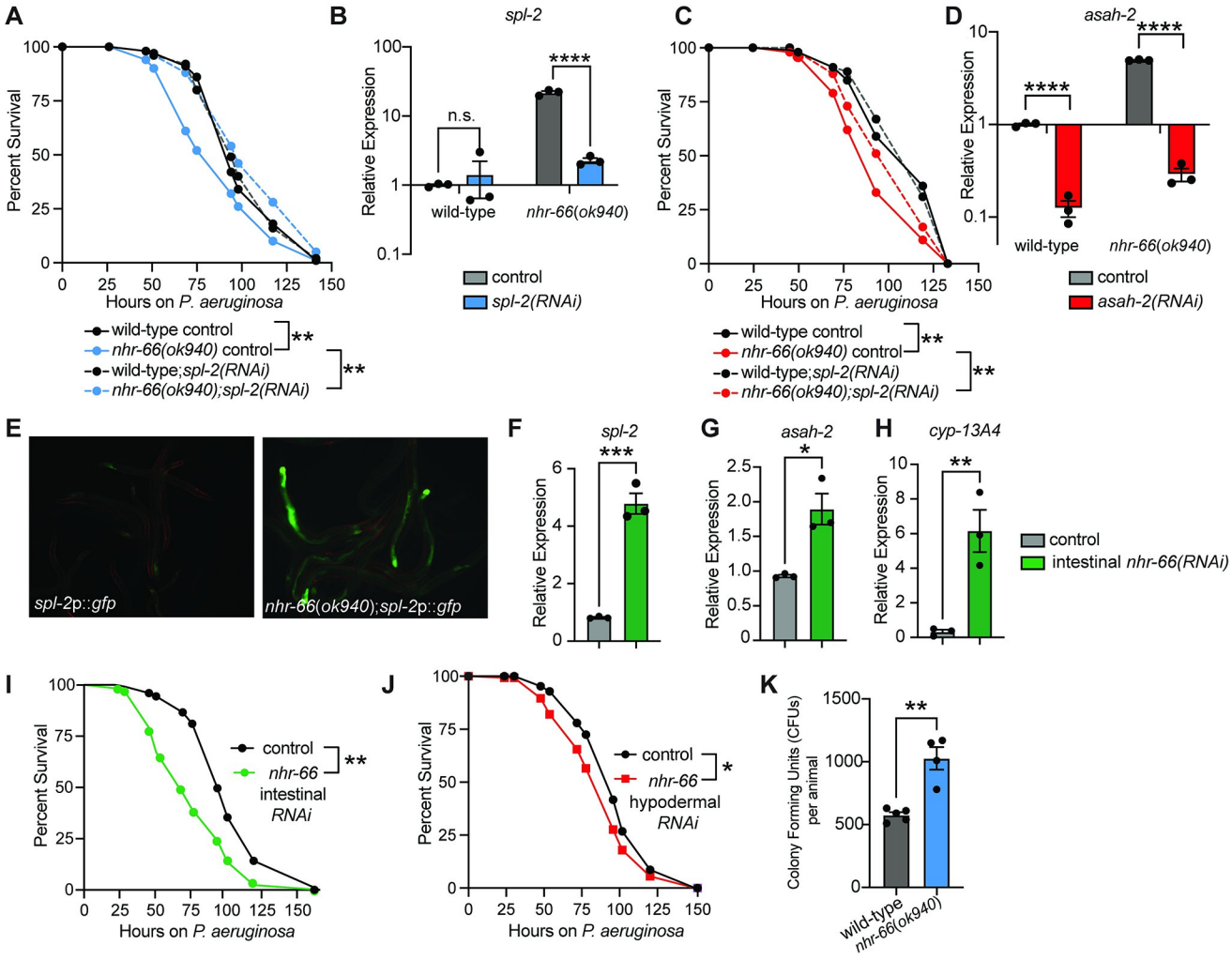

Fig 3. NHR-66 suppresses intestinal sphingolipid catabolism genes to promote resistance to *P. aeruginosa* infection. A–D. *C. elegans-P. aeruginosa* pathogenesis assay with *P. aeruginosa* and *C. elegans* of indicated genotypes at the L4 larval stage are shown (A and C). Differences in survival between *nhr-66(ok940)* mutants and the other genotypes in A and C are significant ** $p<0.01$ (log-rank test). Data representative of three biological replicates ($n = 3$). qRT-PCR analysis of *spl-2* (B) and *asah-2* (D) genes in indicated genetic backgrounds. Data are the average of biological replicates with error bars showing SEM (n = 3). * $p<0.05$, ** $p<0.01$, *** $p<0.001$, **** $p<0.0001$ (two-way ANOVA with Tukey's multiple comparisons test). **E.** Images of *C. elegans spl-2*p::*gfp* animals in wild-type and *nhr-66(ok940)* animals are shown. **F–H.** qRT-PCR analysis of the indicated genes in the indicated genetic backgrounds, as described in B and D. (n = 3) **I and J.** *C. elegans–P. aeruginosa* pathogenesis assays as described above in A and C, except with the indicated genotypes. The difference between the two genotypes in I and J are significant * $p<0.05$, ** $p<0.01$ (log-rank test). Data are representative of two biological replicates (n = 2). **K.** *P. aeruginosa*, isolated from the intestines of animals with the indicated genotypes, were quantified after 24 hours of bacterial infection. Data are colony-forming units (CFU) of *P. aeruginosa* and are presented as the average of 4 separate biological replicates, with each replicate containing 10–11 animals. **equals $p<0.01$ (Student's unpaired t-test). Sample sizes, mean lifespan and p-values for each replicate of the pathogenesis assays in this figure are shown in S5 Table. Other source data for this figure is in S6 Table. Please see also S3 Fig.

https://doi.org/10.1371/journal.ppat.1011730.g003

Sphingolipid degradation in *nhr-66(ok940)* mutants compromises survival during pathogen infection

The NHR-66 targets, *spl-2* and *asah-2* are involved in multiple steps of the sphingolipid degradation pathway (Fig 4A). To determine if NHR-66 regulates sphingolipid breakdown in *C. elegans*, we quantified sphingolipid levels in wild-type and *nhr-66(ok940)* mutants using high-performance liquid chromatography with tandem mass spectrometry (HPLC-MS/MS) (Fig 4B and 4E). We quantified 17 carbon and dihydro-17 carbon sphingolipids, which are the species produced in nematodes [51–53]. In metazoans, sphingolipids are broken down in cells by

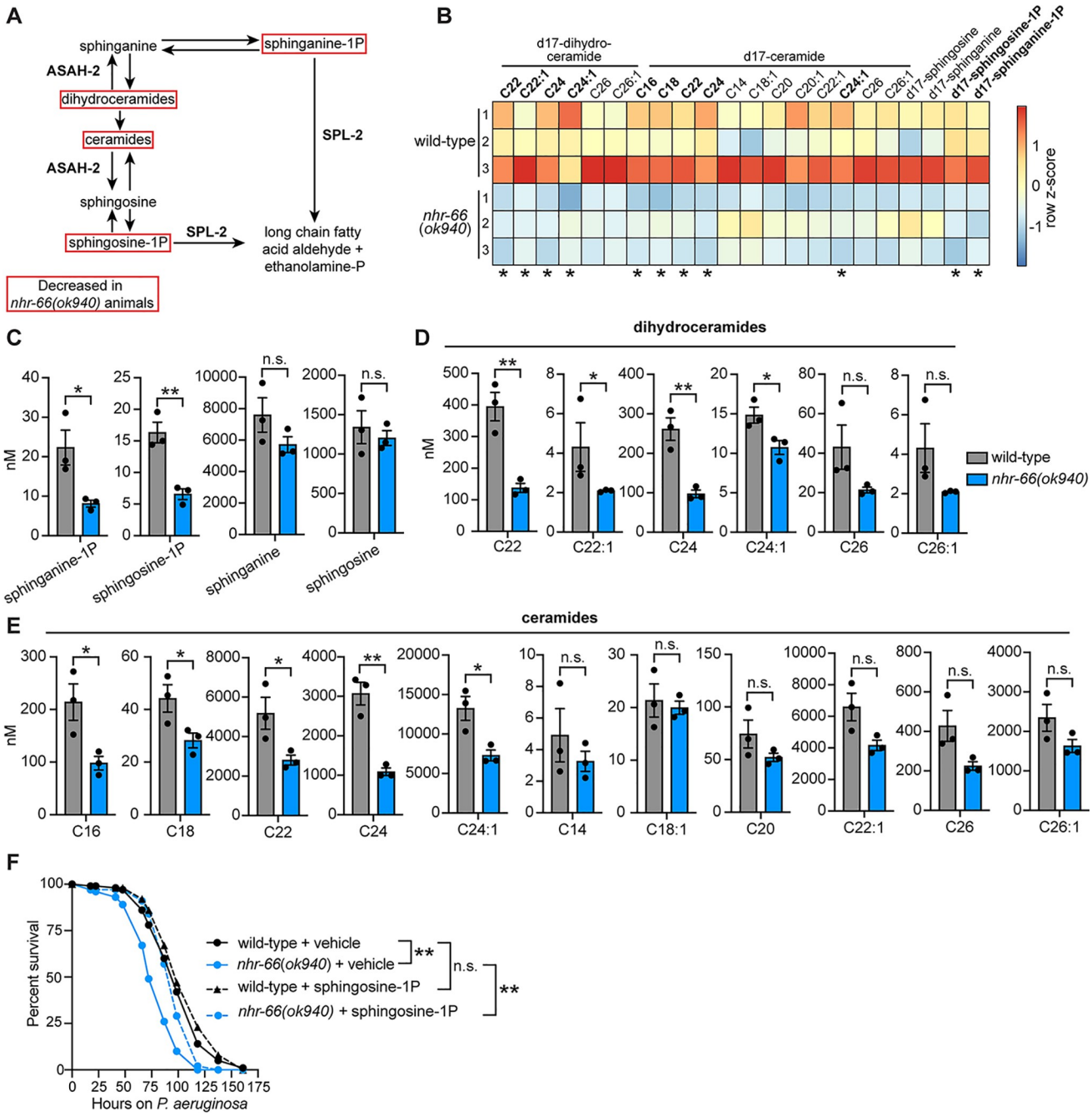

Fig 4. Sphingolipid degradation in *nhr-66(ok940)* mutants compromises survival during pathogen infection. A. Schematic of sphingolipid metabolism in *C. elegans*. **B.** Heatmap of HPLC-MS/MS data depicting the concentrations of d-17 ceramides and di-17 dihydroceramides normalized to total protein levels. The expression level was scaled in each condition by calculating a row z-score for each lipid species $^{*}p<0.05$ (Student's unpaired t-test) **C–E.** The concentrations of the indicated sphingolipids in wild-type versus *nhr-66*(*ok940*) animals as measured by HPLC-MS/MS. n = 3 biological replicates, * $p<0.05$, $^{**}p<0.01$ (Student's unpaired t-test), n.s. (not significant). **F.** *C. elegans-P. aeruginosa* pathogenesis assay with *C. elegans* of indicated genotypes at the L4 larval stage are shown. The difference in survival between *nhr-66(ok940)* mutants and other conditions is significant ** p<0.01 (log-rank test). Data representative of three biological replicates (n = 3). Sample sizes, mean lifespan, and *p*-values for each replicate of this pathogenesis assay are in S5 Table. The source data for this figure is in S6 Table.

https://doi.org/10.1371/journal.ppat.1011730.g004

enzymes that are strongly conserved throughout evolution [54]. Sphingosine phosphate lyase (*C. elegans spl-1* and *spl-2*) and N-acylsphingosine amidohydrolase (also known as acid ceramidase, *C. elegans asah-1* and *asah-2*) function at sequential steps in the sphingosine catabolic pathway (Fig 4A). SPL-1 and SPL-2 catalyze the final, irreversible step in the breakdown of sphingolipids to long-chain fatty acid aldehyde and phospho-ethanolamine (Fig 4A). Thus, consistent with the high levels of SPL-2 expression in *C. elegans nhr-66*(*ok940*) animals, we observed that these mutants had significantly decreased levels of both sphingosine-1-phosphate and sphinganine-1-phosphate (Fig 4A and 4C). The unphosphorylated species sphingosine and sphinganine were unchanged (Fig 4B and 4C), although it is important to note that the levels of these lipids are maintained by both anabolic and catabolic enzymatic reactions (Fig 4A). We also found that the levels of some, but not all, of the sphingolipid species dihydroceramides (Fig 4D) and ceramides (Fig 4E) were lower in *nhr-66(ok940)* mutants, consistent with their enhanced catabolism in this genetic background. In addition, NHR-66 does not regulate the transcription, nor bind to the promoters of paralogs *spl-1* (S3A Fig) or *asah-1* (S3B Fig) Thus, NHR-66 regulates sphingolipid catabolism by repressing the transcription of *spl-2* and *asah-2*, specifically.

Intriguingly, supplementation of sphingosine-1-phosphate, a sphingolipid that is excessively catabolized in the *nhr-66(ok940)* background (Fig 4C), partially rescued the hypersusceptibility of *nhr-66(ok940)* mutants during *P. aeruginosa* infection (Fig 4F). These data indicate that hypersusceptibility of *nhr-66(ok940)* mutants to *P. aeruginosa* infection is secondary to excessive degradation of sphingolipids in this mutant background. It is important to note that sphingosine-1-phosphate can be rapidly converted to other sphingolipids in the cell (Fig 4A). Thus, it is not possible to attribute the enhanced susceptibility of *nhr-66(ok940)* solely to reduced levels of sphingosine-1-phosphate.

In summary, transcriptional de-repression of the sphingolipid catabolism genes *spl-2* and *asah-2* in the *nhr-66(ok940)* mutant background accelerated the breakdown of sphingolipids in a manner that compromised the ability of *C. elegans* to survive bacterial infection. Thus, transcriptional control of sphingolipid catabolism by NHR-66 is necessary for pathogen resistance in *C. elegans*.

NHR-66 and NHR-49 cooperate to regulate sphingolipid metabolism genes

NHR-66 physically interacts with another NHR, the *C. elegans* Peroxisome Proliferator-Activated Receptor (PPAR) homolog (NHR-49), a partnership that has been implicated in the regulation of sphingolipid catabolism genes [49]. NHR-49 is a master regulator of lipid metabolism in *C. elegans* that is also required for survival during pathogen infection [37,38,49,55]. We therefore hypothesized that NHR-49 functions with NHR-66 to promote resistance to *P. aeruginosa*. RNAi-mediated knockdown of *nhr-49* in the *nhr-66(ok940)* mutant background enhanced the susceptibility to pathogen-mediated killing to the same degree as *nhr-49(RNAi)* animals, suggesting that these NHRs cooperate to promote pathogen resistance (Fig 5A). Consistent with these data, and a previous study [56], we found that *nhr-49* and *nhr-66* regulated a significant number of genes in common (Fig 5B), a group that is strongly enriched for metabolism and stress response genes (Fig 5C). Notably, 13 of the 83 genes that are regulated in common by *nhr-49* and *nhr-66* were also among the 18 genes whose promoters were directly bound by NHR-66 in the ChIP-seq experiment (Fig 2A). We examined the transcription of three of these genes (*spl-2*, *asah-2*, and *cyp-13A4*) and observed an additive effect of *nhr-49(RNAi)* and *nhr-66(ok940)* on the expression of *spl-2* (Fig 5D) and *cyp-13A4* (S4 Fig), but not *asah-2* (Fig 5E). Finally, we asked if the hypersusceptibility of *nhr-49* loss-of-function mutants was attributable to the hyper-induction of sphingolipid catabolism genes in this genetic background, as we observed in our studies of *nhr-66* (Fig 3A and 3D). RNAi of *spl-2* (Fig 5F) or *asah-2* (Fig 5G) did not rescue the enhanced susceptibly of *nhr-49(nr2041)* mutants

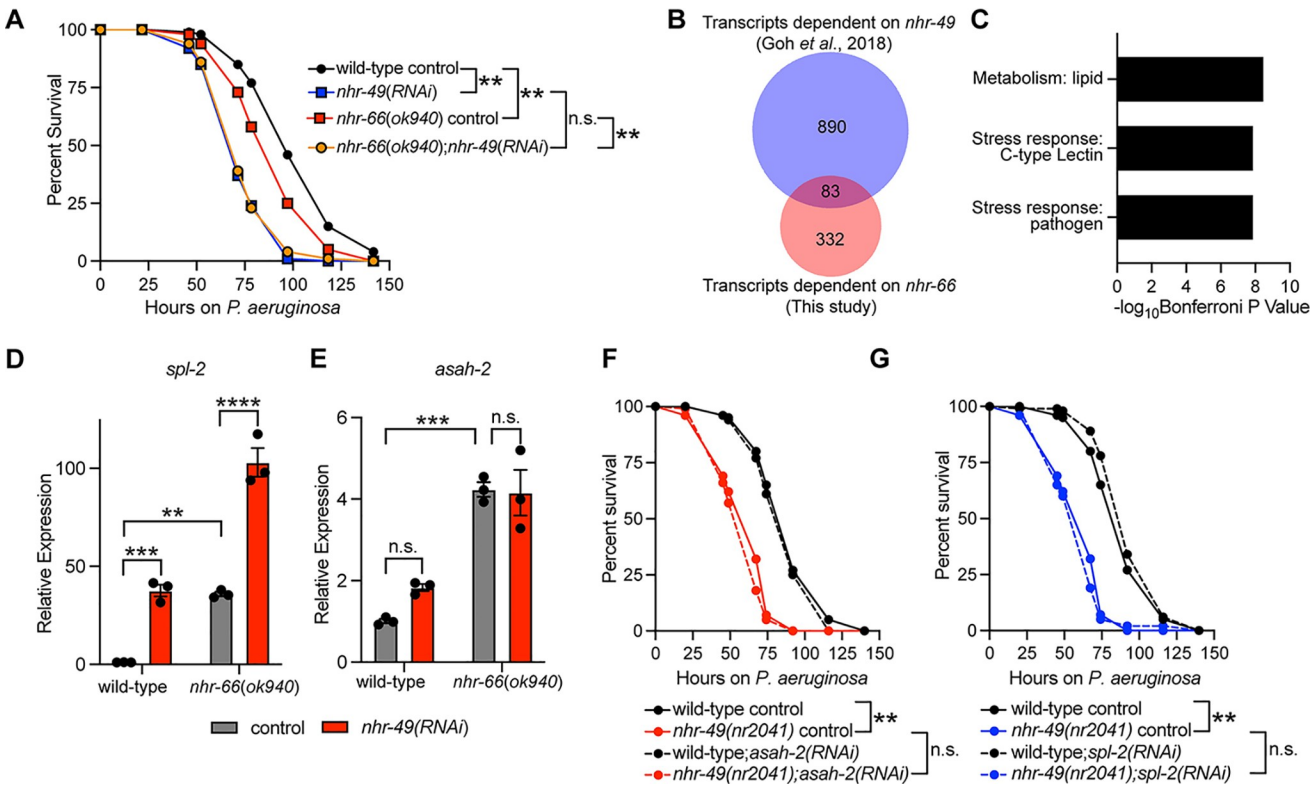

Fig 5. NHR-66 and NHR-49 cooperate to regulate sphingolipid metabolism genes. A. *C. elegans-P. aeruginosa* pathogenesis assay with *C. elegans* of indicated genotypes at the L4 larval stage are shown. Data are representative of three trials. The difference in survival between *nhr-66(ok940)* mutants and *nhr-66(ok940)*; *nhr-49(RNAi)* animals is not significant. The other comparisons are significant ** $p<0.01$ (log-rank test). Data are representative of three biological replicates (n = 3). **B.** Venn diagram showing the overlap between genes that are differentially regulated by *nhr-66* (this study) and those that are differentially regulated by *nhr-49* [56]. The overlap between these datasets is significant (hypergeometric *p*-value = 7.9 x 10^{-26}). See S4 Table. **C.** Gene enrichment analysis for the genes whose transcription are regulated by both *nhr-49* and *nhr-66* is shown. The three most significantly enriched categories are shown, reported as the $\log_{10}$ transformation of the *p*-value for the enrichment of each category. **D and E.** qRT-PCR analysis of the indicated genes in wild-type and *nhr-66(ok940)* mutant animals. Data are the average of three independent replicates with error bars representing SEM. Data are presented as the value relative to the average expression from all replicates of the indicated gene in the baseline condition (wild-type animals exposed to control). ** $p<0.01$, *** $p<0.001$, **** $p<0.0001$ (two-way ANOVA with Tukey's multiple comparisons test). (F and G). *C. elegans-P. aeruginosa* pathogenesis assay with *C. elegans* of indicated genotypes at the L4 larval stage. Difference between *asah-2(RNAi)* (F) or *spl-2(RNAi)* (G) and control RNAi is not significant in wild-type animals but is significant in two out of three trials in *nhr-49(nr2041)* animals. Difference in survival between *nhr-49(nr2041)* and wild-type animals is significant ** $p<0.01$ (log rank). Data are representative of three biological replicates (n = 3). Sample sizes, mean lifespan, and *p*-values for each replicate of the pathogenesis assays in this figure are shown in S5 Table. Other source data for this figure is in S6 Table.

https://doi.org/10.1371/journal.ppat.1011730.g005

to *P. aeruginosa* infection. These data are consistent with previous work, which has established that NHR-49 regulates multiple aspects of host metabolism that are individually important for survival during pathogen infection [37–39,49,55]. In summary, we conclude that NHR-66 and NHR-49 function together to regulate sphingolipid catabolism genes and may cooperate to control pathogen resistance. However, misregulation of sphingolipid metabolism does not by itself account for the hypersusceptibility of *nhr-49* mutants to pathogen infection.

Regulation of sphingolipid catabolism by NHR-66 supports basal, rather than pathogen-induced, host defenses

C. elegans, like other metazoans, coordinate pathogen-inducible immune defenses through mechanisms that detect the pathogen itself or the effects of their secreted toxins. In addition, innate or basal defenses are also required for nematodes to survive challenges from infectious pathogens. Examples in this latter category include structural features of the cell (*e.g.*,

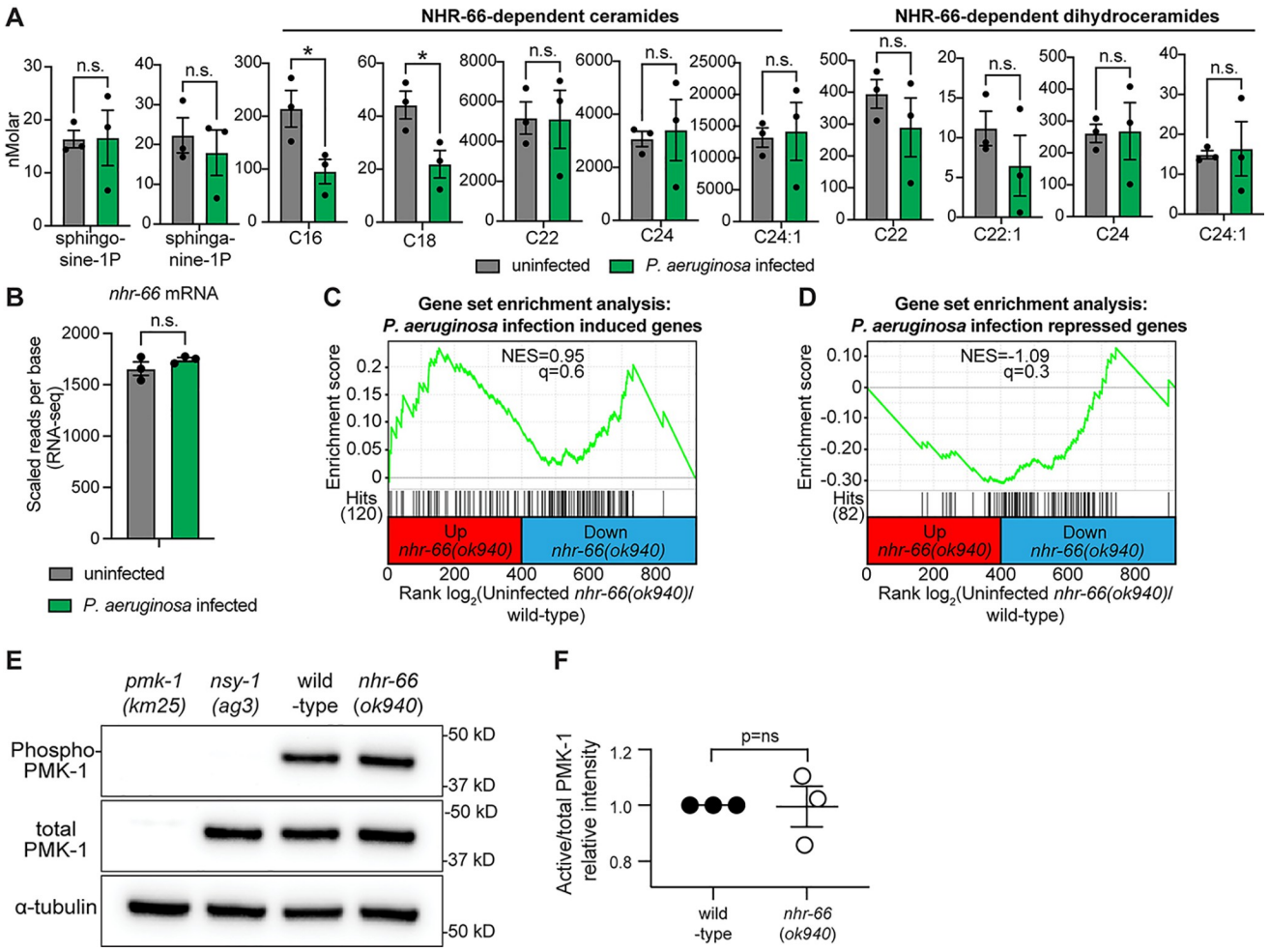

Fig 6. Regulation of sphingolipid catabolism by NHR-66 supports basal, rather than pathogen-induced, host defenses. A. The concentrations of the indicated sphingolipids in wild-type animals either during infection with *P. aeruginosa* or in uninfected controls, as measured by HPLC-MS/MS. Data are the average of three biological replicates with error bars equal to SEM, * $p<0.05$ (Student's unpaired t-test) (n = 3). **B.** RNA-seq data of the *nhr-66* transcript in wild-type animals either during infection with *P. aeruginosa* or in uninfected controls. Data are the average of three biological replicates with error bars equal to SEM. RNAseq data of *C. elegans* infected with *P. aeruginosa* was previously published [41]. **C and D.** Gene set enrichment analysis (GSEA) for genes induced **(C)** or repressed **(D)** in *P. aeruginosa* infected animals in the RNA-seq of *nhr-66* dependent genes. In **(C)** and **(D)**, fold change in the expression of the significantly differentially expressed genes ($q<0.01$) in *nhr-66(ok940)* mutant animals compared to wild-type animals are ranked from higher expression (red) to lower expression (blue). Normalized enrichment score (NES) and q-value are indicated. Genes induced by either condition and found in the *nhr-66(ok940)* transcriptional profile are indicated by hit number in the left margin and black lines. **E.** Immunoblot analysis of lysates from the indicated genotypes probed with antibodies targeting the doubly phosphorylated TGY epitope in phosphorylated PMK-1 (phospho-PMK-1), total PMK-1 protein (total PMK-1), and tubulin (α-tubulin). *nsy-1(ag3)* and *pmk-1(km25)* loss-of-function mutants are the controls, which confirm the specificity of the phospho-PMK-1 probing. **F.** The band intensities of three biological replicates of the Western blot shown in (E) were quantified. Error bars reflect SEM. *equals $p<0.05$ (Student's unpaired t-test). n.s. (not significant). Other source data for this figure is in S6 Table.

https://doi.org/10.1371/journal.ppat.1011730.g006

membranes), the function of organelles, and micronutrients, such as cholesterol. To determine whether the regulation of sphingolipid catabolism by NHR-66 supports pathogen-induced or basal host defenses, we used HPLC-MS/MS to quantify sphingolipid levels in wild-type animals during infection with *P. aeruginosa*. None of the eleven NHR-66-dependent sphingolipids (Fig 4) were upregulated in wild-type animals during infection with *P. aeruginosa*, as might be expected if these sphingolipids were coordinating an inducible response to pathogen infection (Fig 6A). In addition, the transcription of *nhr-66* itself did not change in wild-type animals during *P. aeruginosa* infection (Fig 6B).

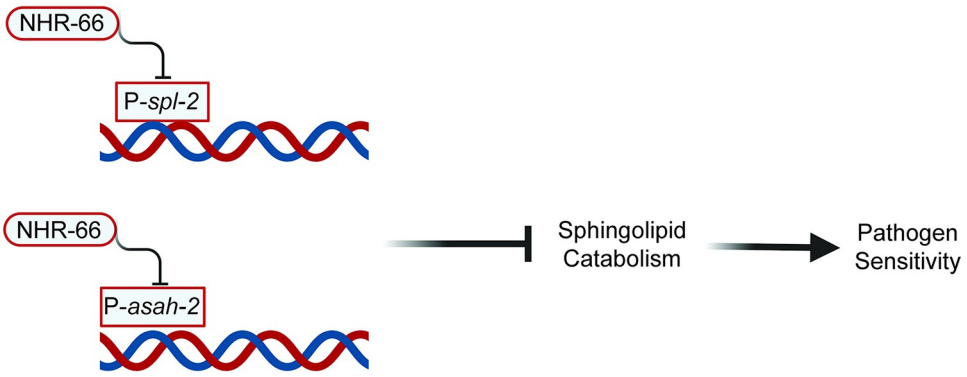

Fig 7. Transcriptional suppression of sphingolipid catabolism controls pathogen resistance in *C. elegans*. Fig 7 was made using BioRender.

https://doi.org/10.1371/journal.ppat.1011730.g007

We next asked if NHR-66 indirectly regulates the transcription of innate immune effectors to promote pathogen resistance (Fig 6C and 6D). In gene enrichment analyses, some genes annotated as pathogen response genes were slightly, but significantly, enriched among the genes that are indirectly regulated by *nhr-66*, both among genes that are expressed lower (S3B Fig) and those that are expressed higher (S3C Fig) in *nhr-66(ok940)* mutants. However, genes that are normally upregulated (Fig 6C) or downregulated (Fig 6D) in wild-type animals during *P. aeruginosa* infection were not overrepresented among *nhr-66*-dependent genes (q = not significant for both comparisons). We also observed that *nhr-66* does not regulate the p38 mitogen-activated protein (MAP) kinase PMK-1 innate immune pathway. The levels of active, phosphorylated p38 PMK-1 were unchanged in *nhr-66*(*ok940*) mutants compared to wild-type animals (Fig 6E and 6F).

Importantly, supplementation of sphingosine-1-phosphate did not appreciably extend the lifespan of wild-type animals during pathogen infection, with a subtle lifespan extension observed in only 2 of 3 biological replicates (Fig 4F), arguing that sphingosine-1-phosphate or a derivative does not activate inducible immune defenses.

We therefore conclude that transcriptional control of sphingolipid catabolism by NHR-66 is required for basal, but not pathogen-inducible, host defense.

Discussion

Sphingolipids play critical roles in cellular physiology. Here we demonstrate that sphingolipid breakdown is regulated at the transcriptional level. We show that *C. elegans* NHR-66 directly regulates sphingolipid catabolism by repressing the transcription of two enzymes, sphingosine phosphate lyase (SPL-2) and acid ceramidase (ASAH-2). Transcriptional repression of these catabolic enzymes by NHR-66 controls the levels of sphingosine-1-phosphate, sphinganine-1-phosphate, and specific ceramides. Control of sphingolipid catabolism, in general, and *spl-2* and *asah-2* regulation specifically, is physiologically important and required for host survival during pathogen challenge. These data define an immunometabolic axis that is necessary for pathogen resistance (Fig 7).

Studies in *C. elegans* have revealed metabolic requirements for host survival during pathogen infection [45]. For example, the monounsaturated fatty acid oleate and the methyl donor S-adenosylmethionine promote innate immunity and pathogen resistance [39,40]. Likewise, insulin/insulin-like growth factor (IGF) signaling, through the insulin/IGF-1 transmembrane receptor homolog DAF-2, integrates nutritional cues and fat utilization to enable survival during bacterial infection [57]. In addition, mobilization of somatic fat to the germline is a protective

response that ensures reproductive fidelity following pathogen challenge [58]. We also previously found that *C. elegans*, which encounter environments scarce in cholesterol, are more susceptible to pathogen-mediated killing and respond by priming innate immune signaling to anticipate threats from virulent bacteria [41]. Thus, a major emerging theme is the utility of the *C. elegans* pathogenesis assays to identify and characterize specific mechanisms of immunometabolism, studies that can be complicated or more challenging in other genetic systems.

Consistent with the important role of sphingolipids in host defense, a previous study found that mutation of the sphingosine kinase *sphk-1* and two putative sphingosine-1-phosphate transporters compromised host survival during *P. aeruginosa* infection [59]. However, it is not known how excess sphingolipid catabolism in the *nhr-66* mutants compromises host survival during pathogen challenge. Our data suggest that sphingolipids are required for basal mechanisms of host defense, but not pathogen-inducible responses, such as those coordinated by soluble signals. This distinction is important because sphingolipids as a group support diverse cellular processes with described functions both as bioactive signaling molecules and key components of cell and organelle membranes. We hypothesize that proper sphingolipid catabolism is important for maintaining membrane integrity, which is required for resistance against pathogens [12,60,61]. Sphingolipids are also important for mitochondrial function, which may be compromised in the *nhr-66* loss-of-function mutants [49,62]. Finally, the pathogen itself may exploit changes in host sphingolipid composition or metabolism to promote its own virulence [63,64]. For example, ethanolamine metabolism in bacteria affects pathogenicity [65–67]. As phospho-ethanolamine is a byproduct of sphingolipid catabolism, increased breakdown of sphingolipids in *nhr-66* loss-of-function mutants may increase the levels of ethanolamine and augment pseudomonal virulence.

C. elegans consume bacteria as their source of nutrition and live in habitats where both infectious pathogens and non-infectious microbes are abundant. Thus, identifying infectious pathogens is particularly challenging for nematodes. Intriguingly, *C. elegans* lost canonical mechanisms of pattern recognition [*e.g.*, Toll-like receptor (TLR) signaling] in evolution, perhaps because TLR ligands (pathogen-associated molecular patterns) are ubiquitous in their environment and are thus insufficient to identify disease-causing pathogens specifically. In this context, we previously proposed that the dramatic expansion of the NHR family in *C. elegans* was fueled, at least in part, by their roles in pathogen detection, immune activation, and immunometabolism [36,68]. In support of this hypothesis, we found that *C. elegans* NHR-86 senses a pathogen-derived metabolite to assess the relative threat of virulent bacteria in the environment and activate innate immunity—a non-canonical mechanism of bacterial pattern recognition [36]. As ligand-gated transcription factors, NHRs are also uniquely positioned to adapt host metabolism to survive challenges from infectious pathogens. In *C. elegans*, for example, NHR-49, the PPARα homolog, is a master regulator of lipid homeostasis that regulates a wide variety of genes involved in the synthesis and utilization of fatty acids and is required to survive pathogen challenge [37,38,48,49]. We observed here that NHR-49 cooperates with NHR-66 to regulate sphingolipid catabolism genes and survival during *P. aeruginosa* infection. These data support a previous study, which found that NHR-49 establishes functional partnerships with NHR-66 and other NHRs to regulate specific metabolic outputs, including genes involved in sphingolipid metabolism [49]. In this context, the ligands of NHR-66 or NHR-49 are not known. It is interesting to note that NHR-66 regulates its own transcription, suggesting that it functions in a feedback loop. Of note, we also report the identification of *nhr-32* from a comprehensive RNAi screen, which is required to resist *P. aeruginosa* infection. We hypothesize that examining the role of diverse pathogens in *C. elegans* will identify a different set of NHRs that survey for virulence-associated metabolites from the pathogen and program adaptive and pathogen-specific changes in host metabolism.

Materials and methods

C. elegans and bacterial strains

The previously published *C. elegans* strains used in this study are: N2 Bristol (wild-type) [69], STE68 *nhr-49*(*nr2041*) [55], AA968 *nhr-8(hd117)* [30], AE501 *nhr-8(ok186)* [70], VC1727 *nhr-32(gk825)* [71], VC1692 *nhr-32(gk810)* [71], KU25 *pmk-1(km25)* [72], *nsy-1(ag3)* [72], MGH167 *sid-1(qt9); alxIs9 [VHA-6*p::*SID-1*::*SL2*::*GFP]* [73], JM43 *(rde-1(ne219); Is [wrt-2*p::*rde-1]* [74], and RB1015 *nhr-66*(*ok940*) [49]. All of these strains were obtained from the *Caenorhabditis* Genetics Center, except KU25, MGH167, and AA968 and JM43, which were obtained from the indicated sources.

The *C. elegans* strains that were developed for this study are: RPW 451 *nhr-66(ums70 [3xFLAG*::*NHR-66])*, RPW 257 *nhr-66*(*ok940*);Fosmid line 1, RPW 257 *nhr-66*(*ok940*);Fosmid line 2, *spl-2*p::*gfp*, *nhr-66*(*ok940*);*spl-2*p::*gfp*, RPW 436 *nhr-32(gk810);umsEx89(nhr-32p*::*FL-nhr32*::*myo-3*::*mCherry)* line 1; RPW 437 *nhr-32(gk810);umsEx90nhr-32p*::*FL-nhr32*::*myo-3*::*mCherry)* line 2, and RPW 280 *nhr-8(hd117);umsEx42(nhr-8p*::*nhr-8*, *myo-2p*::*mCherry) Line 1*, RPW 281 *nhr-8(hd117);umsEx42(nhr-8p*::*nhr-8*, *myo-2p*::*mCherry) Line 2*.

P. aeruginosa strain PA14 was used for all studies [75].

C. elegans bacterial infection and other assays

P. aeruginosa "slow-killing" pathogenesis experiments were performed as previously described [50,76]. The wild-type control for these experiments is N2. Briefly, *P. aeruginosa* PA14 was inoculated into 3 ml of Luria-Bertani (LB) medium and allowed to incubate at 37˚C for 16 hours. Subsequently, 10 μl of this culture was spread onto 35-mm tissue culture plates containing 4 ml of slow-kill agar (0.35% peptone, 0.3% sodium chloride, 1.7% agar, 5 μg/ml cholesterol, 25 mM potassium phosphate, 1 mM magnesium sulfate, 1 mM calcium chloride). Of note, we used peptone from Fisher Scientific for these studies. Plates were incubated for 24 hours at 37˚C, and 24 hours at 25˚C. Twenty minutes before the start of the assay, 0.1 mg/ml 5-fluorodeoxyuridine was added to the medium to prevent progeny from hatching. For all pathogenesis assays that studied *C. elegans* with extrachromosomal arrays, control genotypes, which did not express the array, were obtained from siblings isolated from the same plates as nematodes that contained the array. *C. elegans* lifespan assays were conducted with animals grown on nematode growth media agar at 20˚C in the presence of 40 μg/mL 5-fluoro-2'-deoxyuridine. All pathogenesis and lifespan assays were conducted with nematodes at the L4 larval stage. Unless noted, three independent trials of each pathogenesis assay were performed. Sample sizes, mean lifespan, and *p*-values for all trials are shown in S5 Table.

Colony-forming units of *P. aeruginosa* PA14 were counted in the intestine of *C. elegans* as previously described [50,77]. In brief, *C. elegans* were exposed to *P. aeruginosa* for 24 hours. Animals were then picked to NGM plates lacking bacteria and incubated for 10 minutes to remove external *P. aeruginosa*. Animals were then transferred to a second NGM plate after which 9–11 animals per replicate were collected, washed with M9 buffer containing 25 mM levamisole and 0.01% Triton X-100, and ground with 1.0 mm silicon carbide beads. CFUs were counted from serial dilutions of the lysate.

RNAi screen for *nhr* genes required for pathogen resistance in *C. elegans*

A previously described library containing RNAi clones corresponding to 271 of 274 *nhr* genes in the *C. elegans* genome was used for this study [36,78]. *C. elegans* exposed to each of these RNAi clones were screened for survival on *P. aeruginosa* PA14 following the "slow-kill" protocol described above. In the primary screen, the survival of ~50 animals on a single killing assay

plate was assessed. RNAi clones that caused 0.75 fraction mean survival or greater compared to wild-type were selected and then screened with ~150 animals on three different plates (~50 animals per plate). In the secondary screen, confirmed hits were assayed for lifespan defects by exposing worms to the RNAi clones and transferring them at the L4 stage to non-pathogenic *E. coli* OP50. In the tertiary screen, three independent trials, each with 150 animals, were performed on hits from the secondary screen.

Generation of transgenic *C. elegans* strains

A fosmid containing 31 kb of *C. elegans* DNA (IV:8,209,892..8,240,932), which includes the promoter and coding region for *nhr*-66, as well as for *serp-1.2*, *gpx-6*, *ocr-2*, and C07G1.7, was microinjected into the gonad of *C. elegans nhr-66(ok940)* mutants, and two independent lines that expressed the fosmid in extrachromosomal arrays were recovered. The fosmid was obtained from Source Biosciences. To generate NHR-66::FLAG animals, CRISPR-Cas12 or Cpf-1 editing with single-stranded oligodeoxynucleotide (ssODN) homolog-directed repair was used to knock-in a 3xFLAG sequence at the C-terminus of the *nhr-66* coding sequence, just upstream of the stop codon, as previously described [36,79,80]. The C-terminus was selected for the 3xFLAG knock-in to label all *nhr-66* isoforms. To generate *nhr-32* rescue lines, PCR was used to amplify the entire *nhr-32* locus. The resulting PCR product (10 ng/μL), the *myo-3*p::*mCherry* co-injection marker (15 ng/μL), and pUC19 vector (135 ng/ml) were microinjected into *nhr-32*(*gk810*) animals to generate two independent lines. The list of oligos used in this study is in S7 Table.

Chromatin immunoprecipitation sequencing and bioinformatics

Chromatin immunoprecipitation was performed with a strain containing a 3xFLAG-tagged NHR-66 protein (NHR-66::3x-FLAG) generated in this study, as described above. L4 synchronized hermaphrodite *C. elegans* (wild-type and transgenic NHR-66::3x-FLAG animals) were collected and washed with 4˚C M9 and phosphate-buffered saline to remove bacteria. Cross-linking of protein and DNA was performed in 1% formaldehyde for 10 minutes at room temperature. Cross-linking was quenched with 100 mM glycine, animals were washed in M9, and resuspended in lysis buffer (50 mM Hepes–KOH pH 7.5, 300 mM NaCl, 1 mM EDTA, 1% (v/v) Triton X-100, 0.1% (w/v) sodium deoxycholate, 0.5% (v/v) N-Lauroylsarcosine, and protease inhibitors). Lysates were then sonicated using a Bioruptor UCD-200 for 15 cycles (30s on, 30s off). Anti-flag antibody was pre-incubated with protein G Dynabeads (Invitrogen), and equal amounts of protein from lysate were incubated with 5 μg anti-FLAG antibody (Roche) overnight. 10% of lysate was removed for input. Immune complexes were collected with protein G Dynabeads, washed, and eluted from beads. Cross-links were reversed at 65˚C overnight and DNA fragments were purified with ethanol precipitation. qPCR was performed on input and immunoprecipitated samples using primers designed around the transcription start site. ChIP data are presented as percent input normalized to a random intragenic region on chromosome IV. Primers used for ChIP-PCR studies are in S7 Table.

Deep sequencing of ChIP DNA was performed by Novogene. The raw sequencing data were first clipped for adaptor sequences and then mapped to the *C. elegans* genome (ce11, UC Santa Cruz) by the Burrows-Wheeler Aligner algorithm (BWA MEM, BWA version 0.7.15). The output SAM files were processed and sorted with the Picard tools. The output mapping files (BAM files) were filtered with SAMtools to remove any read that had a mapping quality less than 10 (SAMtools view–b–q 10 input.bam > output.bam). Peaks were determined using MACS version 2.1 with the no-model parameter. The final set of peaks were called if the difference in intensity values of samples had a significance level of p-value < 0.025. ChIP-sequence data is available in S3 Table.

Gene expression analyses and bioinformatics

Approximately 2,500 synchronized *C. elegans* of the indicated genotypes were grown to the L4 stage and harvested by washing with M9. For expression analysis of *C. elegans* genes during *P. aeruginosa* infection, animals at the L4 stage were transferred by washing to plates containing *E. coli* OP50 or *P. aeruginosa* PA14 lawns, prepared as described above. Animals were exposed for four hours and subsequently harvested by washing with M9. RNA was isolated using TriReagent (Ambion), column purified (Qiagen), and analyzed by 150 bp paired-end mRNA-sequencing using the BGI platform (BGI Group) with $>$ 20 million reads per sample. Raw fastq reads were evaluated by FastQC (version 0.11.5), and clean reads were aligned to the *C. elegans* reference genome (WBcel235) and quantified using Kallisto (version 0.45.0) [81]. Differentially expressed genes were identified using Sleuth (version 0.30.0) [82]. Pearson correlation statistical analysis was performed using Prism 9.0. Biological process enrichment was identified using Wormcat [83,84]. Differential gene expression was defined as q less than 0.01. Differentially expressed genes from the RNA-seq experiment are available in S2 Table.

For the qRT-PCR studies, RNA was reverse transcribed to cDNA using the iScript cDNA Synthesis Kit (Bio-Rad Laboratories, Inc.), amplified and detected using SYBR Green (Bio-Rad Laboratories, Inc.) and a CFX384 machine (Bio-Rad Laboratories, Inc.). The sequences of primers that were designed for this study are presented in S7 Table. All values were normalized against the geometric mean of the control genes *snb-1* and *act-3*. Fold change was calculated using the Pfaffl method [85].

Ceramide and sphingolipid profiling

High-performance liquid chromatography with tandem mass spectrometry (HPLC-MS/MS) for quantification of sphingolipid species was performed in the Lipidomics Shared Resource Facility at the Medical University of South Carolina on a Vanquish UHPLC system coupled to a Quantum Access Max triple quadrupole mass spectrometer equipped with an ESI probe operating in the multiple reaction monitoring positive ion mode (Thermo Scientific). Chromatographic separations were obtained under a gradient elution on a C8 column using a mobile phase with ammonium formate, formic acid in water and methanol, as previously described [86]. Prior to analysis, samples underwent an ethyl acetate/isopropanol liquid-liquid extraction. Quantitative analyses of sphingolipids were based on eight-point calibration curves generated for each target analyte. The synthetic standards along with a set of internal standards were spiked into an artificial matrix; they were then subjected to an identical extraction procedure as the biological samples. These extracted standards were then analyzed with the samples by HPLC-MS/MS. Peaks for the target analyses and internal standards were recorded and processed using the instrument's software. Plotting the analyte/internal standard peak area ratios against analyte concentrations was used to generate the sphingolipid-specific calibration curves. Any sphingolipids for which no standards were available were quantitated using the calibration curve of its closest counterpart. Sample sphingolipid levels were normalized to total protein and volume.

Western blots

Protein lysates from *C. elegans* grown to the young L4 larval stage on *E. coli* OP50 on NGM agar were prepared as previously described [36,41]. Briefly, animals were washed three times with M9 buffer, and lysed by sonication in RIPA buffer plus protease and phosphatase inhibitor cocktail. Following centrifugation, protein was quantified from the supernatant of each sample using Bradford Reagent (Bio-Rad Laboratories, Inc.). Laemmli buffer (Bio-Rad Laboratories, Inc.) was added to a concentration of 1X and the total protein from each sample was

resolved on NuPage 4–12% gels (Life Technologies), transferred to nitrocellulose membranes (Life Technologies), blocked with 5% fat-free milk in TBST and probed with a 1:1000 dilution of an antibody that recognizes the doubly-phosphorylated TGY motif of PMK-1 (Cell Signaling Technology) or a monoclonal anti-tubulin antibody (Sigma-Aldrich, Clone B-5-1-2). Horseradish peroxidase (HRP)-conjugated anti-rabbit (Cell Signaling Technology) and anti-mouse IgG secondary antibodies (Abcam) were used at a dilution of 1:10,000 to detect the primary antibodies following the addition of ECL reagents (Thermo Fisher Scientific), which were visualized using a ChemiDoc MP Imaging System (Bio-Rad Laboratories, Inc.).

Microscopy, imaging, and figure preparation

C. elegans were mounted onto 2% agarose pads, paralyzed with 10 mM levamisole (Sigma), and photographed using a Zeiss AXIO Imager Z2 microscope with a Zeiss Axiocam 506 mono camera and Zen 2.3 (Zeiss) software at 10X magnification.

Quantification and statistical analyses

Differences in survival of *C. elegans* in the *P. aeruginosa* pathogenesis assays were determined with the log-rank test after survival curves were estimated for each group with the Kaplan-Meier method. OASIS 2 was used for these statistical analyses [87]. *P*-values were calculated in Prism 9 (GraphPad Software) using one-way ANOVA, unless otherwise indicated in the Fig legend. Sample sizes, mean lifespan, and p-values for all trials are shown in S5 Table.

Supporting information

S1 Fig. An RNAi screen identifies nuclear hormone receptors required for pathogen resistance in *C. elegans*. A and F. Fraction mean survival during *P. aeruginosa* infection of the indicated genotypes. See legend for Fig 1C. * p<0.05 (log rank) in 3 of 3 RNAi biological replicates. **B-E.** *C. elegans-P. aeruginosa* pathogenesis assays, as described for Fig 1E. **p<0.01 (log rank). Related to Fig 1.
(TIF)

S2 Fig. NHR-66 is a transcriptional repressor that binds to promoters. A. Western blot analysis of lysates from wild-type and NHR-66::3xFLAG animals probed with antibodies targeting the FLAG epitope (anti-FLAG) and α-tubulin (anti- tubulin). **B–D.** qRT-PCR analysis of the indicated genes in wild-type and *nhr-66(ok940)* mutant animals. Data are the average of four independent replicates with error bars representing SEM. **$p<0.01$, ****$p<0.0001$ Student's unpaired t-test). Source data for this figure is in S6 Table. Related to Fig 2.
(TIF)

S3 Fig. NHR-66-mediated repression of intestinal sphingolipid catabolism genes promotes pathogen resistance. A-B. ChIP-seq and mRNA-seq profiles from each of the three biological replicates are presented for *spl-1* (A), *and asah-1* (B). The y-axis is the number of reads (log_2). A gene model shows the location of the exons (blue) of the indicated genes. Related to Fig 3.
(TIF)

S4 Fig. NHR-66 and NHR-49 cooperate to regulate sphingolipid metabolism genes. A. qRT-PCR data as described in Fig 5D. *$p<0.05$, ** $p<0.01$, *** $p<0.001$, **** $p<0.0001$ (two-way ANOVA with Tukey's multiple comparisons test). **B and C.** Gene enrichment analyses for the genes whose transcription are indirectly dependent on *nhr-66* is shown. The most significantly enriched categories, reported as the log_{10} transformation of the *p*-value for the enrichment of each category, are shown for genes that are expressed lower (B) and those that are

expressed higher (C) in *nhr-66(ok940)* mutants.
(TIF)

S1 Table. Source data for the RNAi screen for nuclear hormone receptor genes that are required for pathogen resistance in *C. elegans*. Related to Fig 1.
(XLSX)

S2 Table. Data from RNA-seq experiment comparing wild-type to *nhr-66(ok940)* animals. Related to Fig 2.
(XLSX)

S3 Table. Data from ChIP-seq experiment to identify binding targets of NHR-66. Related to Fig 2.
(XLSX)

S4 Table. Overlap of genes regulated by both *nhr-66* and *nhr-49*. Related to Fig 5.
(XLSX)

S5 Table. Sample sizes, mean lifespan, and p values for the *C. elegans* pathogenesis assays. Related to Figs 1E, 3A, 3C, 3I, 3J, 5A, 5G, 5H and S1C–S1E.
(XLSX)

S6 Table. Source data and statistical tests used for each figure and supplemental figure. Related to Figs 1–6 and S1–S4.
(XLSX)

S7 Table. Primer, crRNA guide sequences, and ssODN sequences used in this study. Related to Materials and Methods.
(XLSX)

Acknowledgments

The authors thank Melanie Trombly for critical reading of the manuscript. The authors also thank Gordon Worley, Eduardo Torres, Ryan Palumbo, and Jason Pierce for valuable discussions. Some strains were provided by the Caenorhabditis Genetics Center, which is funded by the NIH Office of Research Infrastructure Programs (P40 OD010440).

Author Contributions

Conceptualization: Mohamad A. Nasrallah, Nicholas D. Peterson, Read Pukkila-Worley.

Data curation: Mohamad A. Nasrallah, Nicholas D. Peterson, Elizabeth S. Szumel, Read Pukkila-Worley.

Formal analysis: Mohamad A. Nasrallah, Nicholas D. Peterson, Elizabeth S. Szumel.

Funding acquisition: Read Pukkila-Worley.

Investigation: Mohamad A. Nasrallah, Nicholas D. Peterson, Elizabeth S. Szumel, Pengpeng Liu, Amanda L. Page, Samantha Y. Tse, Khursheed A. Wani, Claire E. Tocheny.

Methodology: Mohamad A. Nasrallah, Nicholas D. Peterson.

Project administration: Read Pukkila-Worley.

Software: Pengpeng Liu.

Supervision: Read Pukkila-Worley.

Validation: Mohamad A. Nasrallah, Nicholas D. Peterson, Read Pukkila-Worley.

Visualization: Mohamad A. Nasrallah, Nicholas D. Peterson, Pengpeng Liu, Read Pukkila-Worley.

Writing – original draft: Mohamad A. Nasrallah, Read Pukkila-Worley.

Writing – review & editing: Mohamad A. Nasrallah, Nicholas D. Peterson, Read Pukkila-Worley.

References

1. McGinley MP, Cohen JA. Sphingosine 1-phosphate receptor modulators in multiple sclerosis and other conditions. Lancet. 2021; 398: 1184–1194. https://doi.org/10.1016/S0140-6736(21)00244-0 PMID: 34175020
2. Saba JD. Fifty years of lyase and a moment of truth: sphingosine phosphate lyase from discovery to disease. J Lipid Res. 2019; 60: 456–463. https://doi.org/10.1194/jlr.S091181 PMID: 30635364
3. Spiegel S, Milstien S. The outs and the ins of sphingosine-1-phosphate in immunity. Nat Rev Immunol. 2011; 11: 403–415. https://doi.org/10.1038/nri2974 PMID: 21546914
4. Hisano Y, Nishi T, Kawahara A. The functional roles of S1P in immunity. J Biochem. 2012; 152: 305–311. https://doi.org/10.1093/jb/mvs090 PMID: 22923732
5. Pérez-Jeldres T, Alvarez-Lobos M, Rivera-Nieves J. Targeting Sphingosine-1-Phosphate Signaling in Immune-Mediated Diseases: Beyond Multiple Sclerosis. Drugs. 2021; 81: 985–1002. https://doi.org/10.1007/s40265-021-01528-8 PMID: 33983615
6. Bryan AM, Poeta MD. Sphingosine-1-phosphate receptors and innate immunity. Cell Microbiol. 2018; 20: e12836. https://doi.org/10.1111/cmi.12836 PMID: 29498184
7. Aoki M, Aoki H, Ramanathan R, Hait NC, Takabe K. Sphingosine-1-Phosphate Signaling in Immune Cells and Inflammation: Roles and Therapeutic Potential. Mediat Inflamm. 2016; 2016: 8606878. https://doi.org/10.1155/2016/8606878 PMID: 26966342
8. Chi H. Sphingosine-1-phosphate and immune regulation: trafficking and beyond. Trends Pharmacol Sci. 2011; 32: 16–24. https://doi.org/10.1016/j.tips.2010.11.002 PMID: 21159389
9. Mullen TD, Obeid LM. Ceramide and Apoptosis: Exploring the Enigmatic Connections between Sphingolipid Metabolism and Programmed Cell Death. Anti-Cancer Agents Med Chem. 2012; 12: 340–363. https://doi.org/10.2174/187152012800228661 PMID: 21707511
10. Dadsena S, Bockelmann S, Mina JGM, Hassan DG, Korneev S, Razzera G, et al. Ceramides bind VDAC2 to trigger mitochondrial apoptosis. Nat Commun. 2019; 10: 1832. https://doi.org/10.1038/s41467-019-09654-4 PMID: 31015432
11. Liu Z, Xia Y, Li B, Xu H, Wang C, Liu Y, et al. Induction of ER stress-mediated apoptosis by ceramide via disruption of ER Ca2+ homeostasis in human adenoid cystic carcinoma cells. Cell Biosci. 2014; 4: 71. https://doi.org/10.1186/2045-3701-4-71 PMID: 25937892
12. Kraft ML. Sphingolipid Organization in the Plasma Membrane and the Mechanisms That Influence It. Front Cell Dev Biol. 2017; 4: 154. https://doi.org/10.3389/fcell.2016.00154 PMID: 28119913
13. Woodcock J. Sphingosine and ceramide signalling in apoptosis. IUBMB Life. 2006; 58: 462–466. https://doi.org/10.1080/15216540600871118 PMID: 16916783
14. Rudd AK, Devaraj NK. Traceless synthesis of ceramides in living cells reveals saturation-dependent apoptotic effects. Proc Natl Acad Sci. 2018; 115: 7485–7490. https://doi.org/10.1073/pnas.1804266115 PMID: 29967152
15. Lahiri S, Futerman AH. The metabolism and function of sphingolipids and glycosphingolipids. Cell Mol Life Sci. 2007; 64: 2270–2284. https://doi.org/10.1007/s00018-007-7076-0 PMID: 17558466
16. Hwang S, Williams JF, Kneissig M, Lioudyno M, Rivera I, Helguera P, et al. Suppressing Aneuploidy-Associated Phenotypes Improves the Fitness of Trisomy 21 Cells. Cell Rep. 2019; 29: 2473–2488.e5. https://doi.org/10.1016/j.celrep.2019.10.059 PMID: 31747614
17. Coant N, Sakamoto W, Mao C, Hannun YA. Ceramidases, roles in sphingolipid metabolism and in health and disease. Adv Biol Regul. 2017; 63: 122–131. https://doi.org/10.1016/j.jbior.2016.10.002 PMID: 27771292
18. Allende ML, Zhu H, Kono M, Hoachlander-Hobby LE, Huso VL, Proia RL. Genetic defects in the sphingolipid degradation pathway and their effects on microglia in neurodegenerative disease. Cell Signal. 2021; 78: 109879. https://doi.org/10.1016/j.cellsig.2020.109879 PMID: 33296739

19. Platt FM. Sphingolipid lysosomal storage disorders. Nature. 2014; 510: 68–75. https://doi.org/10.1038/nature13476 PMID: 24899306

20. Ballabio A, Bonifacino JS. Lysosomes as dynamic regulators of cell and organismal homeostasis. Nat Rev Mol Cell Bio. 2020; 21: 101–118. https://doi.org/10.1038/s41580-019-0185-4 PMID: 31768005

21. Watson E, Walhout AJM. *Caenorhabditis elegans* metabolic gene regulatory networks govern the cellular economy. Trends Endocrinol Metabolism. 2014; 25: 502 508. https://doi.org/10.1016/j.tem.2014.03.004 PMID: 24731597

22. Giese GE, Nanda S, Holdorf AD, Walhout AJM. Transcriptional regulation of metabolic flux: A *Caenorhabditis elegans* perspective. Curr Opin Syst Biol. 2019; 15: 12–18. https://doi.org/10.1016/j.coisb.2019.03.002

23. Nanda S, Jacques M, Wang W, Myers CL, Yilmaz LS, Walhout AJ. Systems-level transcriptional regulation of *Caenorhabditis elegans* metabolism. Mol Syst Biol. 2023; 19: e11443. https://doi.org/10.15252/msb.202211443 PMID: 36942755

24. Bulcha JT, Giese GE, Ali MdZ, Lee Y-U, Walker MD, Holdorf AD, et al. A Persistence Detector for Metabolic Network Rewiring in an Animal. Cell Rep. 2019; 26: 460–468.e4. https://doi.org/10.1016/j.celrep.2018.12.064 PMID: 30625328

25. Giese GE, Walker MD, Ponomarova O, Zhang H, Li X, Minevich G, et al. *Caenorhabditis elegans* methionine/S-adenosylmethionine cycle activity is sensed and adjusted by a nuclear hormone receptor. eLife. 2020; 9: e60259. https://doi.org/10.7554/elife.60259 PMID: 33016879

26. MacNeil LT, Watson E, Arda HE, Zhu LJ, Walhout AJM. Diet-induced developmental acceleration independent of TOR and insulin in *C. elegans*. Cell. 2013; 153: 240 252. https://doi.org/10.1016/j.cell.2013.02.049 PMID: 23540701

27. Arda HE, Taubert S, MacNeil LT, Conine CC, Tsuda B, Gilst MV, et al. Functional modularity of nuclear hormone receptors in a *Caenorhabditis elegans* metabolic gene regulatory network. Mol Syst Biol. 2010; 6: 367. https://doi.org/10.1038/msb.2010.23 PMID: 20461074

28. Watson E, MacNeil LT, Arda HE, Zhu LJ, Walhout AJM. Integration of metabolic and gene regulatory networks modulates the *C. elegans* dietary response. Cell. 2013; 153: 253 266. https://doi.org/10.1016/j.cell.2013.02.050 PMID: 23540702

29. Watson E, MacNeil LT, Ritter AD, Yilmaz LS, Rosebrock AP, Caudy AA, et al. Interspecies systems biology uncovers metabolites affecting *C. elegans* gene expression and life history traits. Cell. 2014; 156: 759 770. https://doi.org/10.1016/j.cell.2014.01.047 PMID: 24529378

30. Magner DB, Wollam J, Shen Y, Hoppe C, Li D, Latza C, et al. The NHR-8 Nuclear Receptor Regulates Cholesterol and Bile Acid Homeostasis in *C. elegans*. Cell Metab. 2013; 18: 212–224. https://doi.org/10.1016/j.cmet.2013.07.007 PMID: 23931753

31. Sural S, Hobert O. Nematode nuclear receptors as integrators of sensory information. Curr Biology. 2021; 31: 4361–4366.e2. https://doi.org/10.1016/j.cub.2021.07.019 PMID: 34348120

32. Taubert S, Ward JD, Yamamoto KR. Nuclear hormone receptors in nematodes: Evolution and function. Mol Cell Endocrinol. 2011; 334: 49–55. https://doi.org/10.1016/j.mce.2010.04.021 PMID: 20438802

33. Magner DB, Antebi A. *Caenorhabditis elegans* nuclear receptors: insights into life traits. Trends Endocrinol Metabolism. 2008; 19: 153 160. https://doi.org/10.1016/j.tem.2008.02.005 PMID: 18406164

34. Lynch M, Conery JS. The Evolutionary Fate and Consequences of Duplicate Genes. Science. 2000; 290: 1151–1155. https://doi.org/10.1126/science.290.5494.1151 PMID: 11073452

35. Gu Z, Cavalcanti A, Chen F-C, Bouman P, Li W-H. Extent of Gene Duplication in the Genomes of Drosophila, Nematode, and Yeast. Mol Biology Evol. 2002; 19: 256–262. https://doi.org/10.1093/oxfordjournals.molbev.a004079 PMID: 11861885

36. Peterson ND, Tse SY, Huang QJ, Wani KA, Schiffer CA, Pukkila-Worley R. Non-canonical pattern recognition of a pathogen-derived metabolite by a nuclear hormone receptor identifies virulent bacteria in *C. elegans*. Immunity. 2023; 56: 768–782.e9. https://doi.org/10.1016/j.immuni.2023.01.027 PMID: 36804958

37. Naim N, Amrit FRG, Ratnappan R, DelBuono N, Loose JA, Ghazi A. Cell nonautonomous roles of NHR-49 in promoting longevity and innate immunity. Aging Cell. 2021; e13413. https://doi.org/10.1111/acel.13413 PMID: 34156142

38. Wani KA, Goswamy D, Taubert S, Ratnappan R, Ghazi A, Irazoqui JE. NHR-49/PPAR-α and HLH-30/TFEB cooperate for *C. elegans* host defense via a flavin-containing monooxygenase. Elife. 2021; 10: e62775. https://doi.org/10.7554/elife.62775 PMID: 33978570

39. Anderson SM, Cheesman HK, Peterson ND, Salisbury JE, Soukas AA, Pukkila-Worley R. The fatty acid oleate is required for innate immune activation and pathogen defense in *Caenorhabditis elegans*. *Plos Pathog*. 2019; 15: e1007893. https://doi.org/*10.1371/journal.ppat.1007893*

40. Ding W, Smulan LJ, Hou NS, Taubert S, Watts JL, Walker AK. s-Adenosylmethionine Levels Govern Innate Immunity through Distinct Methylation-Dependent Pathways. Cell Metab. 2015; 22: 633 645. https://doi.org/10.1016/j.cmet.2015.07.013 PMID: 26321661

41. Peterson ND, Icso JD, Salisbury JE, Rodríguez T, Thompson PR, Pukkila-Worley R. Pathogen infection and cholesterol deficiency activate the *C. elegans* p38 immune pathway through a TIR-1/SARM1 phase transition. eLife. 2022; 11: e74206. https://doi.org/10.7554/elife.74206 PMID: 35098926

42. Otarigho B, Aballay A. Cholesterol regulates innate immunity via nuclear hormone receptor NHR-8. Iscience. 2020; 23: 101068. https://doi.org/10.1016/j.isci.2020.101068 PMID: 32361270

43. Goswamy D, Gonzalez X, Labed SA, Irazoqui JE. *C. elegans* orphan nuclear receptor NHR-42 represses innate immunity and promotes lipid loss downstream of HLH-30/TFEB. Front Immunol. 2023; 14: 1094145. https://doi.org/10.3389/fimmu.2023.1094145 PMID: 36860863

44. Rajan M, Anderson CP, Rindler PM, Romney SJ, Santos MCF dos, Gertz J, et al. NHR-14 loss of function couples intestinal iron uptake with innate immunity in *C. elegans* through PQM-1 signaling. Elife. 2019; 8: e44674. https://doi.org/10.7554/elife.44674 PMID: 31532389

45. Anderson SM, Pukkila-Worley R. Immunometabolism in *Caenorhabditis elegans*. PLoS Pathog. 2020; 16: e1008897. https://doi.org/10.1371/journal.ppat.1008897 PMID: 33031414

46. Hahn-Windgassen A, Gilst MRV. The *Caenorhabditis elegans* HNF4α Homolog, NHR-31, Mediates Excretory Tube Growth and Function through Coordinate Regulation of the Vacuolar ATPase. PLoS Genet. 2009; 5: e1000553. https://doi.org/10.1371/journal.pgen.1000553 PMID: 19668342

47. Sim S, Hibberd ML. *Caenorhabditis elegans* susceptibility to gut *Enterococcus faecalis* infection is associated with fat metabolism and epithelial junction integrity. Bmc Microbiol. 2016; 16: 6. https://doi.org/10.1186/s12866-016-0624-8 PMID: 26769134

48. Dasgupta M, Shashikanth M, Gupta A, Sandhu A, De A, Javed S, et al. NHR-49 Transcription Factor Regulates Immunometabolic Response and Survival of *Caenorhabditis elegans* during *Enterococcus faecalis* Infection. Infect Immun. 2020; 88: e00130–20. https://doi.org/10.1128/iai.00130-20 PMID: 32482643

49. Pathare PP, Lin A, Bornfeldt KE, Taubert S, Gilst MRV. Coordinate Regulation of Lipid Metabolism by Novel Nuclear Receptor Partnerships. Plos Genet. 2012; 8: e1002645. https://doi.org/10.1371/journal.pgen.1002645 PMID: 22511885

50. Foster KJ, McEwan DL, Pukkila-Worley R. Measurements of Innate Immune Function in *C. elegans*. Methods Mol Biology Clifton N J. 2020; 2144: 145–160. https://doi.org/10.1007/978-1-0716-0592-9_13 PMID: 32410032

51. Chitwood DJ, Lusby WR, Thompson MJ, Kochansky JP, Howarth OW. The glycosylceramides of the nematode *Caenorhabditis elegans* contain an unusual, branched-chain sphingoid base. Lipids. 1995; 30: 567–573. https://doi.org/10.1007/bf02537032 PMID: 7651085

52. Cheng X, Jiang X, Tam KY, Li G, Zheng J, Zhang H. Sphingolipidomic Analysis of *C. elegans* reveals Development- and Environment-dependent Metabolic Features. Int J Biological Sci. 2019; 15: 2897–2910. https://doi.org/10.7150/ijbs.30499 PMID: 31853226

53. Hannich JT, Mellal D, Feng S, Zumbuehl A, Riezman H. Structure and conserved function of iso-branched sphingoid bases from the nematode *Caenorhabditis elegans*. Chem Sci. 2017; 8: 3676–3686. https://doi.org/10.1039/c6sc04831e PMID: 30155209

54. Abe A, Shayman JA. Encyclopedia of Biological Chemistry (Second Edition). Lipids Carbohydr Membr Membr Proteins: Artic Titles: S. 2013; 287–292. https://doi.org/10.1016/b978-0-12-378630-2.00462-x

55. Gilst MRV, Hadjivassiliou H, Jolly A, Yamamoto KR. Nuclear hormone receptor NHR-49 controls fat consumption and fatty acid composition in *C. elegans*. O'Rahilly S, editor. Plos Biol. 2005; 3: e53. https://doi.org/10.1371/journal.pbio.0030053 PMID: 15719061

56. Goh GYS, Winter JJ, Bhanshali F, Doering KRS, Lai R, Lee K, et al. NHR-49/HNF4 integrates regulation of fatty acid metabolism with a protective transcriptional response to oxidative stress and fasting. Aging Cell. 2018; 17: e12743. https://doi.org/10.1111/acel.12743 PMID: 29508513

57. Troemel ER, Chu SW, Reinke V, Lee SS, Ausubel FM, Kim DH. p38 MAPK Regulates Expression of Immune Response Genes and Contributes to Longevity in *C. elegans*. PLoS Genet. 2006; 2: e183. https://doi.org/10.1371/journal.pgen.0020183 PMID: 17096597

58. Nhan JD, Turner CD, Anderson SM, Yen C-A, Dalton HM, Cheesman HK, et al. Redirection of SKN-1 abates the negative metabolic outcomes of a perceived pathogen infection. Proc National Acad Sci. 2019; 201909666. https://doi.org/10.1073/pnas.1909666116 PMID: 31611372

59. Lee K, Escobar I, Jang Y, Kim W, Ausubel FM, Mylonakis E. In the Model Host *Caenorhabditis elegans*, Sphingosine-1-Phosphate-Mediated Signaling Increases Immunity toward Human Opportunistic Bacteria. Int J Mol Sci. 2020; 21: 7813. https://doi.org/10.3390/ijms21217813 PMID: 33105563

60. Bollinger CR, Teichgräber V, Gulbins E. Ceramide-enriched membrane domains. Biochim Biophys Acta (BBA)—Mol Cell Res. 2005; 1746: 284–294. https://doi.org/10.1016/j.bbamcr.2005.09.001 PMID: 16226325

61. Merrill AH. Sphingolipid and Glycosphingolipid Metabolic Pathways in the Era of Sphingolipidomics. Chem Rev. 2011; 111: 6387–6422. https://doi.org/10.1021/cr2002917 PMID: 21942574

62. Liu Y, Samuel BS, Breen PC, Ruvkun G. *Caenorhabditis elegans* pathways that surveil and defend mitochondria. Nature. 2014; 508: 406 410. https://doi.org/10.1038/nature13204 PMID: 24695221

63. Wang J, Chen Y-L, Li Y-K, Chen D-K, He J-F, Yao N. Functions of Sphingolipids in Pathogenesis During Host–Pathogen Interactions. Front Microbiol. 2021; 12: 701041. https://doi.org/10.3389/fmicb.2021.701041 PMID: 34408731

64. Okino N, Ito M. Molecular mechanism for sphingosine-induced *Pseudomonas* ceramidase expression through the transcriptional regulator SphR. Sci Rep-uk. 2016; 6: 38797. https://doi.org/10.1038/srep38797 PMID: 27941831

65. Coutinho BG, Mevers E, Schaefer AL, Pelletier DA, Harwood CS, Clardy J, et al. A plant-responsive bacterial-signaling system senses an ethanolamine derivative. Proc Natl Acad Sci. 2018; 115: 9785–9790. https://doi.org/10.1073/pnas.1809611115 PMID: 30190434

66. Lundgren BR, Sarwar Z, Pinto A, Ganley JG, Nomura CT. Ethanolamine Catabolism in *Pseudomonas aeruginosa* PAO1 Is Regulated by the Enhancer-Binding Protein EatR (PA4021) and the Alternative Sigma Factor RpoN. J Bacteriol. 2016; 198: 2318–2329. https://doi.org/10.1128/jb.00357-16 PMID: 27325678

67. Garsin DA. Ethanolamine utilization in bacterial pathogens: roles and regulation. Nat Rev Microbiol. 2010; 8: 290–295. https://doi.org/10.1038/nrmicro2334 PMID: 20234377

68. Peterson ND, Cheesman HK, Liu P, Anderson SM, Foster KJ, Chhaya R, et al. The nuclear hormone receptor NHR-86 controls anti-pathogen responses in *C. elegans*. Plos Genet. 2019; 15: e1007935. https://doi.org/10.1371/journal.pgen.1007935 PMID: 30668573

69. Brenner S. The Genetics of *Caenorhabditis elegans*. Genetics. 1974; 77: 71–94. https://doi.org/10.1093/genetics/77.1.71 PMID: 4366476

70. Lindblom TH, Pierce GJ, Sluder AE. A *C. elegans* orphan nuclear receptor contributes to xenobiotic resistance. Curr Biology. 2001; 11: 864–868. https://doi.org/10.1016/s0960-9822(01)00236-6 PMID: 11516648

71. Gene: *nhr-32*, Species: *Caenorhabditis elegans*—Caenorhabditis Genetics Center (CGC)—College of Biological Sciences. [cited 7 Aug 2023]. Available: https://cgc.umn.edu/gene/nhr-32

72. Kim DH, Feinbaum R, Alloing G, Emerson FE, Garsin DA, Inoue H, et al. A conserved p38 MAP kinase pathway in *Caenorhabditis elegans* innate immunity. Science. 2002; 297: 623 626. https://doi.org/10.1126/science.1073759 PMID: 12142542

73. Zhou B, Kreuzer J, Kumsta C, Wu L, Kamer KJ, Cedillo L, et al. Mitochondrial Permeability Uncouples Elevated Autophagy and Lifespan Extension. Cell. 2019; 177: 299–314.e16. https://doi.org/10.1016/j.cell.2019.02.013 PMID: 30929899

74. Zugasti O, Bose N, Squiban B, Belougne J, Kurz CL, Schroeder FC, et al. Activation of a G protein-coupled receptor by its endogenous ligand triggers the innate immune response of *Caenorhabditis elegans*. Nat Immunol. 2014; 15: 833 838. https://doi.org/10.1038/ni.2957 PMID: 25086774

75. Rahme LG, Stevens EJ, Wolfort SF, Shao J, Tompkins RG, Ausubel FM. Common Virulence Factors for Bacterial Pathogenicity in Plants and Animals. Science. 1995; 268: 1899–1902. https://doi.org/10.1126/science.7604262 PMID: 7604262

76. Tan M-W, Mahajan-Miklos S, Ausubel FM. Killing of *Caenorhabditis elegans* by *Pseudomonas aeruginosa* used to model mammalian bacterial pathogenesis. Proc National Acad Sci. 1999; 96: 715–720. https://doi.org/10.1073/pnas.96.2.715 PMID: 9892699

77. Foster KJ, Cheesman HK, Liu P, Peterson ND, Anderson SM, Pukkila-Worley R. Innate Immunity in the *C. elegans* Intestine Is Programmed by a Neuronal Regulator of AWC Olfactory Neuron Development. Cell Reports. 2020; 31: 107478. https://doi.org/10.1016/j.celrep.2020.03.042 PMID: 32268082

78. MacNeil LT, Pons C, Arda HE, Giese GE, Myers CL, Walhout AJM. Transcription Factor Activity Mapping of a Tissue-Specific in vivo Gene Regulatory Network. Cell Syst. 2015; 1: 152 162. https://doi.org/10.1016/j.cels.2015.08.003 PMID: 26430702

79. Dokshin GA, Ghanta KS, Piscopo KM, Mello CC. Robust Genome Editing with Short Single-Stranded and Long, Partially Single-Stranded DNA Donors in *Caenorhabditis elegans*. Genetics. 2018; 210: 781–787. https://doi.org/10.1534/genetics.118.301532 PMID: 30213854

80. Ghanta KS, Mello CC. Melting dsDNA Donor Molecules Greatly Improves Precision Genome Editing in *Caenorhabditis elegans*. Genetics. 2020; 216: 643–650. https://doi.org/10.1534/genetics.120.303564 PMID: 32963112

81. Bray NL, Pimentel H, Melsted P, Pachter L. Near-optimal probabilistic RNA-seq quantification. Nat Biotechnol. 2016; 34: 525–527. https://doi.org/10.1038/nbt.3519 PMID: 27043002

82. Pimentel H, Bray NL, Puente S, Melsted P, Pachter L. Differential analysis of RNA-seq incorporating quantification uncertainty. Nat Methods. 2017; 14: 687–690. https://doi.org/10.1038/nmeth.4324 PMID: 28581496

83. Holdorf AD, Higgins DP, Hart AC, Boag PR, Pazour GJ, Walhout AJM, et al. WormCat: An Online Tool for Annotation and Visualization of *Caenorhabditis elegans* Genome-Scale Data. Genetics. 2020; 214: 279–294. https://doi.org/10.1534/genetics.119.302919 PMID: 31810987

84. Higgins DP, Weisman CM, Lui DS, D'Agostino FA, Walker AK. Defining characteristics and conservation of poorly annotated genes in *Caenorhabditis elegans* using WormCat 2.0. Genetics. 2022; 221: iyac085. https://doi.org/10.1093/genetics/iyac085 PMID: 35587742

85. Pfaffl MW. A new mathematical model for relative quantification in real-time RT–PCR. Nucleic Acids Res. 2001; 29: e45–e45. https://doi.org/10.1093/nar/29.9.e45 PMID: 11328886

86. Bielawski J, Pierce JS, Snider J, Rembiesa B, Szulc ZM, Bielawska A. Sphingolipids as Signaling and Regulatory Molecules. Adv Exp Med Biol. 2010; 688: 46–59. https://doi.org/10.1007/978-1-4419-6741-1_3 PMID: 20919645

87. Han SK, Lee D, Lee H, Kim D, Son HG, Yang J-S, et al. OASIS 2: online application for survival analysis 2 with features for the analysis of maximal lifespan and healthspan in aging research. Oncotarget. 2016; 7: 56147–56152. https://doi.org/10.18632/oncotarget.11269 PMID: 27528229